EVALUATION OF THOR-50M, WORLDSID-50M AND GHBMC M50-O v6.0 MODLES IN FAR-SIDE CRASHES

Jay Zhao
Deepak Vasant Sabannavar
Mutaz Shkoukani
Joyson Safety Systems
United States

Paper Number 23-0283

ABSTRACT

This study is conducted to assess biofidelity of three occupant models (GHBMC human 50th%ile male occupant model M50-O v6.0, Humanetics male THOR dummy model v1.8.1 and WorldSid-50M model v7.6) in far-side crash test conditions and to better understand the kinematics and response of a far-side mid-sized driver in a compact size vehicle crashed to a 285° oblique right-side rigid pole at 31.01 km/h (NHTSA FMVSS 214 Test # 210915).

Far-side occupant simulations for various sled and vehicle crash tests have been conducted. Firstly, the GHBMC human body model (HBM) is correlated with the three post-mortem human subjects (PMHS) far-side sled tests performed by University of Virginia (UVA) [1] at two crash severities and two impact directions. Secondly, a series of the far-side sled test simulations with paired HBM and anthropomorphic test device (ATD) cases are conducted, varying with severities and impact directions, seats, and central console presence. Lastly, occupant simulations are performed for a belted far-side mid-size male driver, represented by the HBM and the WorldSid-50M model respectively, in the subject compact passenger car in the FMVSS 214 pole test. Comparative analysis is made for the kinematics and responses of the HBM and the WorldSid-50M model at the vehicle crash.

The HBM correlation results show that the GHBMC M50-O v6.0 human model reasonably correlates well with the PMHS kinematics and response from the 60-degree oblique far-side UVA sled tests. The HBM estimated high injury risk for the thorax is in line with the post-test PMHS injury outcomes.

The comparative HBM-ATD studies at both the far-side sled tests and the vehicle pole crash test indicate that both ATD models have positive and negative biofidelity outcomes compared to the HBM. The THOR dummy has similar head/neck/torso kinematic and response measures compared to the HBM under the oblique sled test conditions, while its pelvis and lower leg respond poorly to the lateral inertia loads. The WorldSid-M50 dummy model has the whole-body kinematics similar to the HBM under the oblique sled test conditions, while it shows stiffer lateral bending of the torso and smaller chest deflections than the HBM especially under the lateral far-side loadings.

The subject vehicle side crash test occupant simulation with the HBM predicts that the mid-size male driver may suffer severe injuries on the chest and moderate injuries on the head and abdomen.

INTRODUCTION

According to 2020 European New Car Assessment Programme (Euro NCAP) statements, side impacts account for around a quarter of all crashes. In a lateral/side impact, the occupants on both the struck (near) side and on the opposite (far) side of the vehicle are at risk of injury. Earlier study by Digges et al. [2] on the NASS/CDS 1988-98 indicated that fatality risk in far-side oblique collisions was comparable to that in near-side collisions. The head accounted for 45% of the MAIS 4+ injuries in far-side collisions and the chest/abdomen accounted for 39%. Yoganandan et al. [3] found that the abdominal injuries especially to the liver and spleen also occurred often in far-side collisions. Gabler et al. [4] investigated over 100 cases of Australian far side struck occupants from the MIDS database, and over 4500 cases of U.S. far side struck occupants from NASS/CDS 1993-2002. They found that far side struck occupants have a significant risk of injury in both Australia and the United States. As a fraction of all occupants who experienced a side impact, far side struck occupants accounted for approximately 20% of the

seriously injured persons and 25-29% of the Harm. Bahouth et al [5] studied the NASS CDS 2004-2013 data. The results indicated that far-side oblique collisions were the most common impact direction caused serious injuries. The chest/abdominal injuries accounted for 43% and head injuries accounted for 23% of the AIS 3+ injuries. Drivers accounted for 79% of the MAIS 3+ injured belted front outboard occupants that were involved in far-side crashes. About 53% of front outboard occupant's chest injuries were caused by contacts with the vehicle center stack or seat back and 21% were associated with contacts with the far-side structure. More than 60% of the AIS 3+ head injuries were caused by the far side structure. Of the far-side crash involved occupants analyzed, they sustained AIS3+ head or chest injuries from the far side of the vehicle more than 4.4 times more often than were attributed to occupant to occupant contact. Hostetler et al. [6] recently queried NASS/CDS 2000–2015 dababase resulted in 4495 non-weighted far-side crashes. For AIS 2+ through 5+ injury, the injury risks increased 2.48-3.66% per delta-V increase of 11.9 kph. Multiple impacts were significant factors on increased AIS 3+ through 5+ injuries. For AIS 2+ body region injuries, lateral delta-V and maximum CDC extent were positively associated with increased head, thorax, and lower extremity injury risk while belt use was associated with lower risk.

Far-side crashes are expected to increase in near future as more new automated vehicles (AV) are in the field. The trends in AV interior seating configurations bring more innovative and versatile design options than the conventional vehicles. Other than the traditional forward-facing seats, AV seating designs may have seating positions of oblique-facing, rear-facing, and side facing or the other angle-oriented. The oblique and side-facing seat positions will become far-side like collision environment in the frontal or side collisions observed often from the field.

Better protection of far-side occupants in crashes requires better test protocol and injury evaluation tools. Extensive reaserch and development have been conducted in the past decades. Recently, Euro NCAP [7] regulates a new far side occupant test & assessment procedure that details the assessments to be performed in far side occupant protection that contribute to the side impact part of the adult occupant protection rating. Far side protection is assessed using two sled tests that are representative of AE-MDB and Oblique Pole test configurations. One WorldSID 50th male dummy will be seated on the far side of the vehicle. In addition, data from full-scale testing is required to demonstrate head protection countermeasures for occupant-to-occupant interaction.

The advanced anthropomorphic test devices like WorldSID-50M dummy and THOR male dummy have been developed. Biofidelity of these ATDs are evaluated from various studies. Particularly for the far-side applications, Pintar et al. [8] performed far-side sled tests at both low (11 km/h) and high (30 km/h) velocities for six PMHS and the THOR and the WorldSID dummies. Their matched-pair comparisons for the kinematics and responses among post-mortem human subjects (PMHS), WorldSID, and THOR-NT indicated both positive and negative biofidelity outcomes for both the THOR and the WorldSID dummies in the far-side crash mode. Forman et al. [1] performed a series of far-side lateral and oblique sled tests with seven PMHS. With this set of test data biofidelity of GHBMC M50-O v4.4 model was assessed [11]. Biofidelity of the THOR 50th percentile male dummy was evaluated by Parent et al. [9] for the frontal impacts. However, its biofidelity particularly for the far-side applications are not yet fully understood. Rhule et al. [10] evaluated biofidelity of WorldSid-50M dummy using an updated biofidelity ranking system. The data showed that the WorldSID dummy demonstrated Internal Biofidelity values of 1.4 and External Biofidelity values of 2.2 (with Abdomen). For the body regions of thorax and pelvis, the WorldSID dummy received an overall external BioRank score of 3.2 and 2.7 respectively, indicative of improvement required for the pendulum force response measurement of the oblique pendulum impact test.

With the most recent advances in development of more biofidelic human occupant surrogates, new generation of human body models and FE models of advanced ATDs have been under development. The Global Human Body Model Consortium (GHBMC) has developed recently the 50th percentile male occupant model (named as GHBMC AM50-O v6.0). The Humanetics male THOR dummy model v1.8.1 and WorldSid-50M v7.6, validated with multiple component and system impact tests, have been used in the industry as the digital "twins" of the dummy hardware. Nevertheless, research questions as follows still remain:

1) Is biofidelity of the GHBMC AM50-O v6.0 HBM good for applications in far-side crashes?
2) How are the kinematics, responses and injury measures of Humanetics male THOR dummy model v1.8.1 comparable to the HBM at oblique far-side sled test conditions?
3) How are the kinematics, responses and injury measures of WorldSid-50M dummy model v7.6 comparable to the HBM at various far-side sled and vehicle crash test conditions?

This study is aimed to address those questions to assess and identify appropriate occupant model(s) for evaluation of restraint performance and far-side occupant's kinematics, responses, and injury risks.

METHODS

This study is conducted in three phases.

Phase 1: **HBM validation** to assess biofidelity of the HBM (GHBMC M50-O v6.0 model) via the model correlation with the far-side sled tests data provided by University of Virginia (UVA) [1].

Phase 2: **Far-side sled test occupant simulations** for parametric comparative analysis for a far-side mid-size male occupant at various sled test conditions. The two ATD models — Humanetics male THOR dummy model v1.8.1 and WorldSid-50M model v7.6 are compared respectively with the validated HBM from the results of ATD-HBM paired cases.

Phase 3: **Vehicle crash far-side occupant simulations** for the kinematics and responses of a far-side mid-size occupant in the subject compact passenger car right side pole crash, in which the kinematics and responses of WorldSid-50M model v7.6 are compared to the HBM.

HBM Correlation with PMHS Tests

To compare the GHBMC AM50-O v6.0 HBM to the PMHS in the far-side collisions, three UVA PMHS far-side sled tests [1] with variation of impact severity and angle are simulated. Table 1 lists the simulation matrix I for the HBM correlation with the UVA sled tests, in which the PMHS 602 was tested at 60-degree oblique loadings with the 14g and 6.6g pulses respectively, and the PMHS 559 was tested at the 90-degree loading with the 14g pulse.

Table 1.
Simulation matrix I: the UVA far-side sled tests for the HBM correlation

Case #	Case Name	Test Number	PMHS#	Delta V (km/h)	Impact Direction to Occupant	Pretensioner	Arm Position	D-ring Position
C1	HM134	S0134	602	15	60 Deg	Yes	Down	Intermediate
C2	HM135	S0135	602	32	60 Deg	Yes	Down	Intermediate
C3	HM091	S0091	559	32	90 Deg	Yes	Down	Intermediate

Table 2 summarizes information of the PMHS in the tests and the HBM in the simulations. The GHBMC AM50-O v6.0 model represents a male occupant of 77 kg weight, 175 cm tall and BMI of 25.1.

Table 2.
PMHS and GHBMC AM50-O v6.0 model information

Occupant	Mass (kg)	Stature (cm)	BMI	Age
PMHS-602 (oblique)	79	178	24.9	61
PMHS-559 (lateral)	73	175	23.8	60
GHBMC AM50-O	77	175	25.1	-

Figure 1 shows the HBM simulation model per the UVA PMHS far-side sled tests setup.

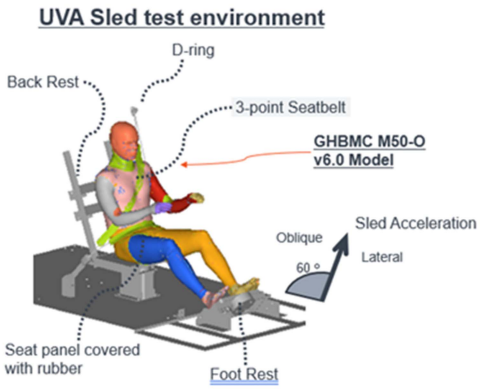

Figure 1. UVA PMHS far-side sled test model.

The base sled test model is from the validated one used in our previous study [11] for GHBMC M50-O v4.4 model. It consists of the FE models of the base sled, the base seat and the seatbelt that were built based on the physical geometries and properties of the UVA far-side sled test fixture [1]. The D-Ring position and the shoulder belt routing for the positioned HBM are set up per each the PMHS test.

In the update PMHS far-side sled test model, the GHBMC AM50-O v6.0 model is swapped in the base sled test model. The newly replaced HBM is individually positioned to match the initial locations of head, torso, pelvis, knee, and ankle targets of each PMHS in each test after performing a series of positioning pre-simulations that followed same procedure as the previous study [11]. Table 3 compares the initial positions between the HBM and the PMHS in terms of six position measurements in the sagittal plane: distance between H-point and the seat front edge; distance between D-ring to the seat front edge; angle between D-ring and left shoulder; angle between T3 and L1 (Torso Angle); angle between H-point and knee (Femur Angle); and angle between knee and ankle (Tibia Angle). All the measurements are matched well between the HBM and the PMHS except for the H-point to seat distance, for which matching H-point position is given a lower priority over matching the pelvis CG and head CG locations.

Table 3.
PMHS/HBM position measurements

Case #	Case Name	Subject	H-pt. to Seat (mm)	D-ring to Seat (mm)	Belt Angle (deg)	Torso Angle (deg)	Femur Angle (deg)	Tibia Angle deg)
C1	HM134	PMHS-602	119	525	44	80	14	43
		HBM 134	81	525	45	76	13	45
C2	HM135	PMHS-602	118	521	48	81	12	47
		HBM 135	81	521	45	76	13	45
C3	HM091	PMHS-559	118	521	48	81	12	47
		HBM 091	81	521	45	76	13	45

Far-side Sled Test Occupant Simulations

Specific purposes of this phase of study are defined as

(i) to assess biofidelity of each ATD (the THOR-M50 and WorldSid-M50) by comparing the kinematics and responses to the HBM from each ATD-HBM paired case, and

(ii) to evaluate trends of the kinematics and injury measures variation with various far-side sled test conditions.

Table 4 defines simulation matrix II for the ATD-HBM parametric comparative study. Twelve simulation cases in total are defined, among which Cases C2 and C3 belonging to the simulation matrix I (Table I) are included for completeness. There are seven paired ATD-HBM simulation cases defined below:

(i) Cases C2-HM135 vs. C6-TR138 — paired HBM-THOR at the oblique sled with the UVA steel seat,

(ii) Cases C4-HM136 vs. C7-TR139 — paired HBM-THOR at the oblique sled with the production seat,

(iii) Cases C5-HM137 vs. C8-TR140 — paired HBM-THOR at the oblique sled with the production seat and a right-side console,

(iv) Cases C2-HM135 vs. C9-WS141 —paired HBM-WORLDSID at the oblique sled with the UVA steel seat,

(v) Cases C4-HM136 vs. C10-WS142 — paired HBM-WORLDSID at the oblique sled with the production seat,
(vi) Cases C5-HM137 vs. C11-WS143 — paired HBM-WORLDSID at the oblique sled with the production seat and a right-side console, and
(vii) Cases C3-HM091 vs. C12-WS144 — paired HBM-WORLDSID at the 90 deg side sled with the UVA steel seat.

The simulation case setup with the UVA steel seat without seat console is per the UVA PMHS sled tests [1], for which Cases C2, C3, C6, C9, and C12 are included. For the other cases in the matrix II, the simulated sled test configurations for the seating environment are different from the UVA sled tests, where the steel seat is replaced a validated generic FE production seat model and presence of a generic console is considered.

Table 4.
Simulation matrix II: Far-side sled test simulation cases for ATD-HBM comparative analysis

Case #	Case Name	Crash Pulse or Condition	O-Model	Seat	Seat Console
C2	HM135	UVA Far side Oblique,14g	M50-O v6.0	UVA Steel Seat	No
C3	HM091	UVA Far side 90Deg,14g	M50-O v6.0	UVA Steel Seat	No
C4	HM136	UVA Far side Oblique,14g	M50-O v6.0	Production Seat	No
C5	HM137	UVA Far side Oblique,14g	M50-O v6.0	Production Seat	Yes
C6	TR138	UVA Far side Oblique,14g	THOR v1.8.1	UVA Steel Seat	No
C7	TR139	UVA Far side Oblique,14g	THOR v1.8.1	Production Seat	No
C8	TR140	UVA Far side Oblique,14g	THOR v1.8.1	Production Seat	Yes
C9	WS141	UVA Far side Oblique,14g	WSID v7.6	UVA Steel Seat	No
C10	WS142	UVA Far side Oblique,14g	WSID v7.6	Production Seat	No
C11	WS143	UVA Far side Oblique,14g	WSID v7.6	Production Seat	Yes
C12	WS144	UVA Far side 90Deg,14g	WSID v7.6	UVA Steel Seat	No
C13	WS145	UVA Far side 90Deg,14g	WSID v7.6	Production Seat	No

The HBM positioning at Cases C4 and C5 is same as C2, for which the position measurements are summarized in Table 3. The THOR dummy model positioned at Cases C6-C8 is set to match the HBM case C2 for the initial locations of head, torso, pelvis, knee, and ankle targets. The WorldSID dummy model positioned at Cases C9-C11 is per the HBM position C2 and positioned at C12-C13 is per the HBM position C3. Table 5 summarizes the (X, Y, Z) coordinates of the head CG, left and right shoulder, pelvis CG, left and right knee and ankle targets of the HBM, THOR, and WorldSID dummy models for all the cases listed in Table 4.

Table 5.
Coordinates (X, Y, Z) of the positioning targets of the occupant models in Cases C2-C13

O-Model	Case Name	Head CG (X,Y,Z)	Left Shoulder Target (X,Y,Z)	Right Shoulder Target (X,Y,Z)	Pelvis CG (X,Y,Z)	Left Knee Target (X,Y,Z)	Right Knee Target (X,Y,Z)
M50-O v6.0	HM135, HM136, HM137	(-103, 0, -761.8)	(-103, -234, -492)	(-103, 234, -492)	(-1, 0, -95)	458, -205, -146)	(458, 205, -146)
THOR v1.8.1	TR138, TR139, TR140	(-101, 0, -782)	(-104, -235, -538)	(-104, 235, -538)	(-48, 0, -92)	(456, -200, -149)	(456, 200, -149)
WSID v7.6	WS141, WS142, WS143	(-87, 0, -759)	(-126, -245, -507)	(-126, 245, -507)	(-81, 0, -92)	(460, -217, -194)	460, 217, -194)
M50-O v6.0	HM091	(-88, 0, -769)	(-109, -237, -492)	(-109, 237, -492)	(-132, 0, -91)	(413, -190, -147)	(413, 190, -147)
WSID v7.6	WS144, WS145	(-86, 0, -761)	(-138, -245, -511)	(-138, 245, -511)	(-98, 0, -108)	(435, -203, -167)	(435, 203, -167)

Figure 2 shows three sled test simulation models variants with each of the occupant models – the HBM, the THOR model v1.8.1 and the WorldSid model v7.6.

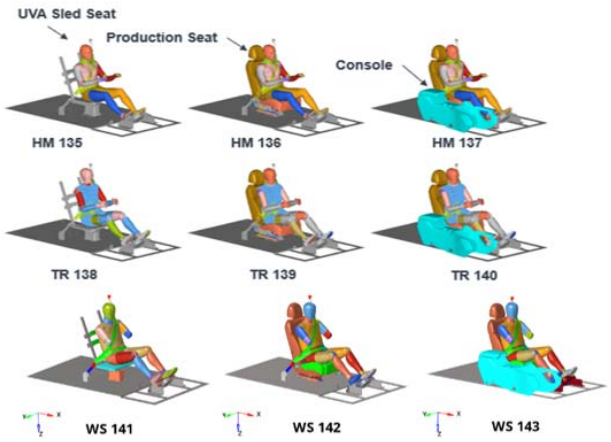

Figure 2. HBM/ATD far-side sled test simulation models setup.

Vehicle Crash Far-side Occupant Simulations

The simulated subject vehicle was a compact passenger car crashed in the FMVSS 214 rigid pole right side impact test conducted by the Transportation Research Center Inc. in East Liberty, Ohio, USA on September 15, 2021 (NHTSA test# 210915). In the test the vehicle was towed into the rigid pole at an angle of 285° with a velocity of 31.01 km/h.

A 2010 Toyota Yaris FE model is downloaded from crash simulation vehicle models database managed by National Crash Analysis Center (NCAC). This FE vehicle model is then updated to represent the subject vehicle. Modifications are made for the exterior and interior body parts (such as body, door and door trims etc.), morphed based on the reported pre-test dimension measurement data from the test for the case vehicle. The maximum deformation of right-side door and door-trims are profiled per the post-test measured right-side door intrusion data. The 1st row seatbelt/pretensioner and anchorage attachments and the driver and passenger seats are represented by the same FE component models used in the sled test simulations in the matrix II, while the 2nd row seat is not included. The driver and passenger seats are repositioned per the reported seat measurement data from the test. The subject vehicle CG location and value are adjusted to match the measurement data from the test. The measured vehicle CG three-dimensional accelerations and vehicle pitch, yaw and roll velocities from the test are imposed by prescribed motion to the subject vehicle model.

The other interior parts surround the 1st row occupants, specifically the full facia assembly consisting of the facia, steering column, and steering wheel as well as the knee bolsters and floors, remain same as the original vehicle model. The full tunnel/central console components consisting of the full tunnel trim, hand brake assembly, gear lever assembly and storage compartments from the original vehicle model are labeled as the "Center Console 1" option for the evaluation.

The simulated far-side occupant is a mid-sized male occupant seating on the driver side, represented by the GHBMC M50-O v6.0 HBM and the Humanetics WorldSid-50M dummy model v7.6 respectively. Each occupant model is positioned same in the vehicle per the reported dummy's longitudinal and lateral clearance dimensions measurement from the test.

Table 6 defines simulation matrix III including two far-side occupant simulation cases for the subject vehicle pole crash.

Table 6.
Simulation matrix III: Cases for the far-side occupant in the subject compact car from NHTSA FMVSS214 pole crash test

Case #	Case Name	LHS Occupant	Seat	Center Console	Far-side AB
C14	HM146	HBM v6.0	Production Seat	Center Console 1	None

C15	WS147	WSID v7.6	Production Seat	Center Console 1	None

Figure 3 shows the far-side occupant simulation model with the subject vehicle for the two cases.

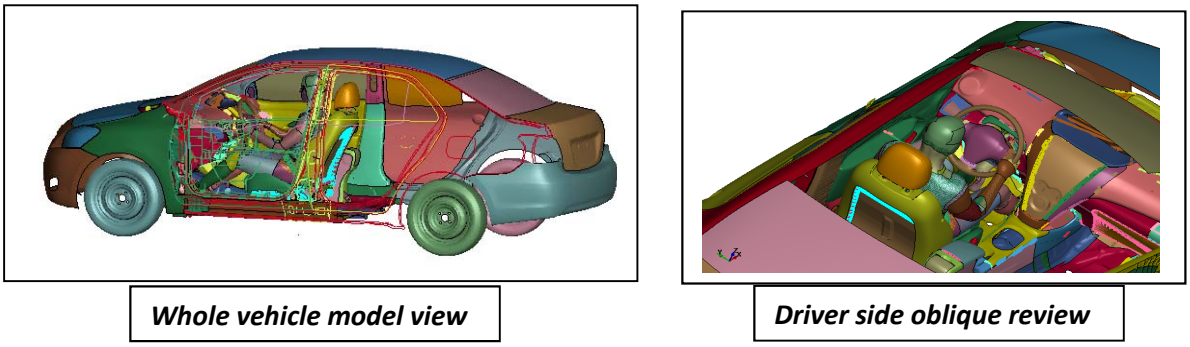

Figure 3. The far-side occupant simulation models for the two cases of the subject vehicle right side pole crash.

Data Analysis and Processing

The data processing and analysis are performed for all the simulation cases for the three occupant models of GHBMC M50-O model v6.0, Humanetics THOR model v1.8.1, and Humanetics WorldSid-50M model v7.6.

The following outputs and measurements are processed for both the HBM and the ATD models:

- the head CG accelerations and rotational velocities,
- the forces and moments of the upper neck, lower neck and spine (T12),
- the shoulder forces and shoulder rib deflections (for WorldSID and HBM),
- the accelerations of T1, T4, T12 and pelvis CG,
- the chest and abdomen deflections at all the measurement locations of each ATD (THOR or WorldSID and comparable outputs from the HBM),
- the forces and moments of the pubic, acetabulum, and the left & right femur,
- the relative displacements (to the seat) of the kinematics targets or Vicon targets of the head, left and right shoulder (acromion), T1, T4, T12, pelvis, left and right knees.

The response and injury measures are normalized with the normalization values in Table 7 that are defined for the HBM and the ATDs separately based on the criterion that each pair of the HBM-ATD have about same estimated injury risk for same body region.

Table 7.
Normalization Values for HBM/THOR/WorldSID Injury Measures

Body Region	Measure	HBM Normalization Value	Risk	THOR Normalization Value	Risk	WSID Normalization Value	Risk
Head	HIC15	800	15%	800	15%	800	15%
	BrIC	1	56%	1	56%	1	56%
Neck	NIJ (Upper)	1	35%	1.3	34%	1	35%
	NIJ (Lower)	1	NA	1.5	NA	1.5	NA
	Tension (Upper) (kN)	4.17	25%	4.17	NA	4.17	NA
	Extension (Upper) (Nm)	25	NA	35	NA	35	NA
	Lateral Bend (Upper) (Nm)	100	NA	150	NA	150	NA
	Tension (Lower) (kN)	4.17	NA	4.17	NA	4.17	NA
	Extension (Lower) (Nm)	25	NA	35	NA	35	NA
	Lateral Bend (Lower) (Nm)	100	NA	150	NA	150	NA
Thorax	T4 G 3ms (G)	60	NA	60	NA	60	NA
	L Shoulder Joint Force (kN)	2	NA	2.25	NA	2.25	48%
	R Shoulder Joint Force (kN)	2	NA	2.25	NA	2.25	48%
	L Shoulder Rib Def (mm)	68	51%	--	NA	40	51%
	R Shoulder Rib Def (mm)	68	51%	--	NA	40	51%
	L. Upper Chest Def (mm)	68	51%	52	51%	40	51%

	R. Upper Chest Def (mm)	68	51%	52	51%	40	51%
	L. Mid Chest Def (mm)	68	51%	--	51%	40	51%
	L. Low Chest Def (mm)	68	51%	52	51%	40	51%
	R. Mid Chest Def (mm)	68	51%	--	51%	40	51%
	R Low Chest Def (mm)	68	51%	52	51%	40	51%
Abdomen	L Upper ABD Def (mm)	75	48%	95	46%	50	48%
	R Upper ABD Def (mm)	75	48%	95	46%	50	48%
	L Low ABD Def (mm)	75	48%	NA	46%	50	48%
	R Low ABD Def (mm)	75	48%	NA	46%	50	48%
Pelvis	Pubic Force (kN)	3.1	49%	--	NA	2.35	49%
	L. Accetab Force (kN)	3.45	NA	3.45	48%	6	NA
	R. Accetab Force (kN)	3.45	NA	3.45	48%	6	NA
Knee-Thigh	L. Femur Force (kN)	14	40%	10	43%	10	43%
	R. Femur Force (kN)	14	40%	10	43%	10	43%

The injury risks for the body regions of head, neck, thorax, abdomen, pelvis, and knee-thigh are calculated separately for the 50th%ile male HBM, WorldSID-50M, and THOR using the published injury risk functions [12-20] tabulated in Table A-1, A-2 & A-3 in Appendix A, respectively.

The Occupant Injury Measure (OIM_{AIS3+}^{ATD}) for the AIS 3+ injury risk estimated from the ATDs or HBM was calculated by (1)

$$OIM_{AIS3+}^{ATD} = 1-(1-P_{HIC})*(1-P_{BrIC})*\left(1-Max(P_{NIJ},P_{NeckFz+},P_{NeckFz-})\right)*(1-P_{ChCD})*\left(1-P_{ABDef}\right)*(1-P_{PeivisF})*(1-P_{FemurF}) \quad \textbf{(Equation 1)}$$

where P_{HIC}, P_{BrIC}, $P_{NIJ}, P_{NeckFz+}, P_{NeckFz-}$, $P_{ChCD}, P_{ABDef}, P_{PeivisF}, P_{FemurF}$ are the AIS 3+ injury probabilities calculated with the measures of Head Injury Criterion (HIC15) and Brain Injury Criterion (BrIC), Neck Injury Criterion (NIJ) and Neck Tension Forces, Chest Deflections, Abdomen Deflections, Pelvic Forces, and Femur Force, respectively.

RESULTS

HBM Test Correlation Results

Case C1: HM134 with 6.6g pulse at 60-deg

Figure 5 shows snapshots of the GHBMC M50-O model v6.0 HBM kinematics compared to the PMHS -602 video from the UVA far-side sled test S0134 (6.6g pulse in 60deg). The kinematics of the HBM is similar to the PMHS.

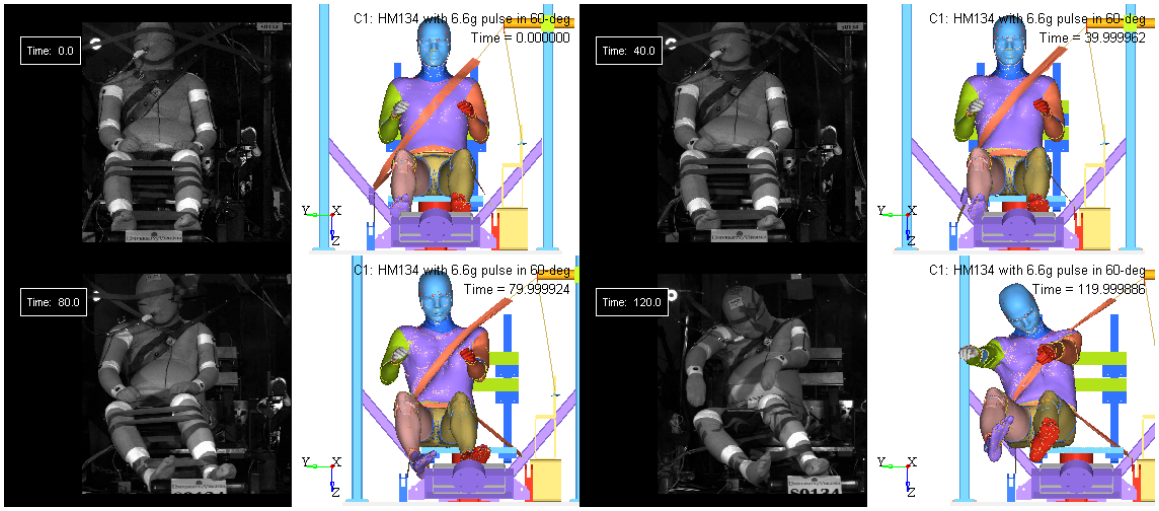

Figure 5. Snapshots of the GHBMC M50-O model v6.0 kinematics compared to the PMHS -602 video from the UVA sled test S0134 (6.6g pulse at 60deg) at 0msec, 40msec, 80 msec, and 120msec (Courtesy: The PMHS test data provided by UVA).

Figure 6 shows correlations of the time-histories of the responses and kinematics target displacements (relative to the seat) of the GHBMC M50-O model v6.0 against the measured censor signals and Vicon data of PMHS -602 from the UVA oblique far-side sled test S0134 (6.6g pulse at 60deg). Good correlations are seen for this sled test condition.

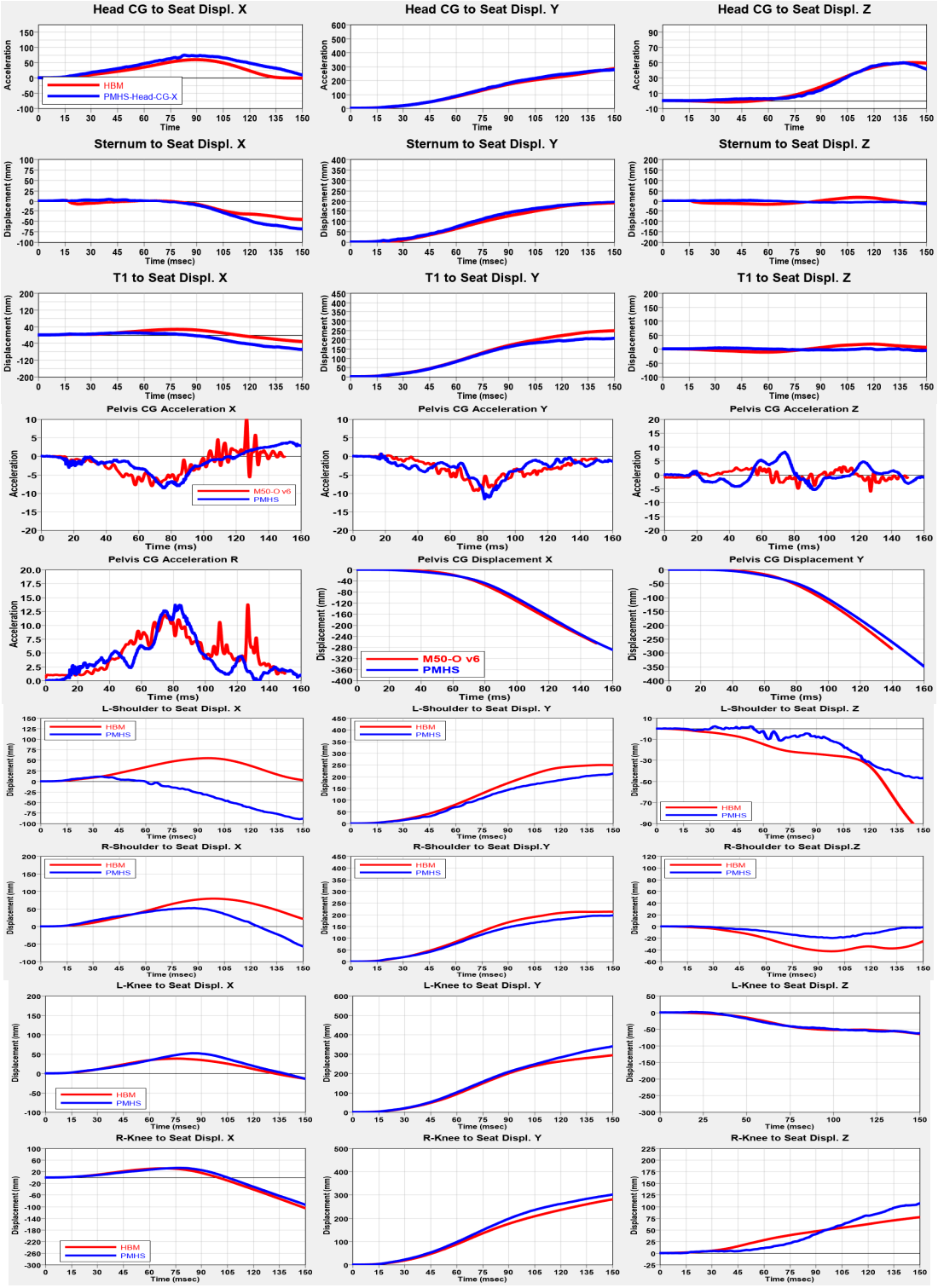

Figure 6. The time-histories of responses and kinematics target displacements of the GHBMC M50-O model v6.0 (red curve) compared to the test data of PMHS -602 (blue curve) from the UVA oblique far-side sled test S0134 (6.6g pulse at 60deg). (Courtesy: The PMHS test data provided by UVA).

<u>Case C2: HM135 with 14g pulse at 60-deg</u>

Figure 7 compares snapshots of the HBM kinematics to the PMHS -602 video from the UVA far-side sled test S0135 (14g pulse in 60deg) at 0msec, 40msec, 80msec and 120msec. The HBM kinematics looks like the PMHS for this test condition as well.

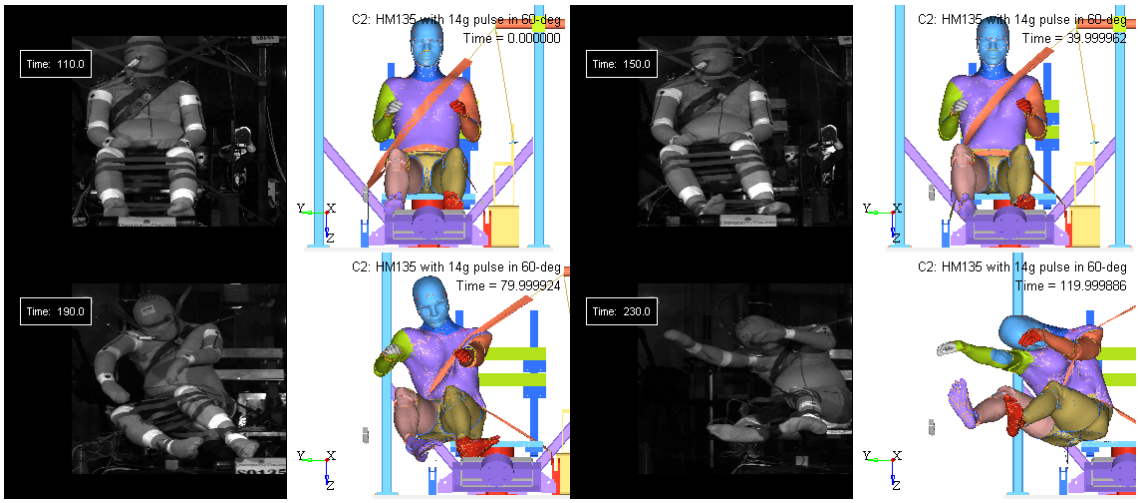

Figure 7. Snapshots of the GHBMC M50-O model v6.0 kinematics compared to the PMHS -602 video from the UVA sled test S0135 (14g pulse at 60deg) at 0msec, 40msec, 80 msec, and 120msec (Courtesy: The PMHS test data provided by UVA).

Figure 8 shows the time-histories of the relative displacements of the HBM head, sternum, T1, pelvis, left and right shoulders and knees compared to the Vicon data of PMHS -602 from the UVA oblique far-side sled test S0135 (14 pulse in 60deg). Overall, the HBM target displacements are close to the PMHS.

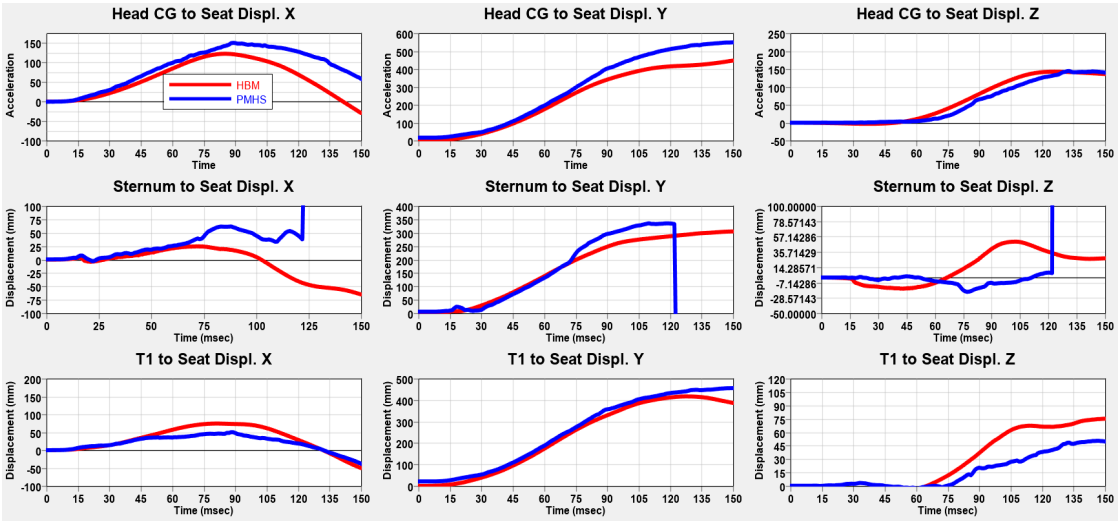

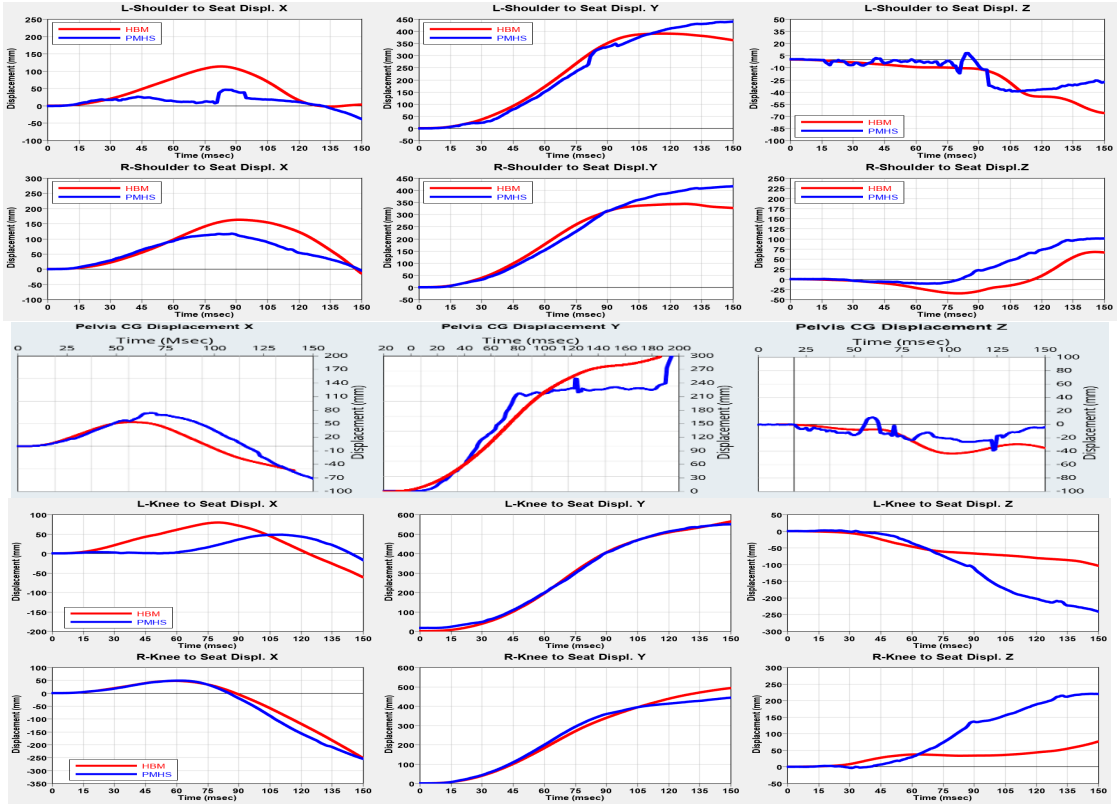

Figure 8. The time-histories of kinematics target relative-to-seat displacements of the GHBMC M50-O model v6.0 (red curve) compared to the test data of PMHS -602 (blue curve) from the UVA oblique far-side sled test S0135 (14g pulse at 60deg). (Courtesy: The PMHS test data provided by UVA).

<u>Case C3: HM091 with 14g pulse in 90-deg</u>

Figure 9 shows snapshots of the GHBMC M50-O model v6.0 kinematics compared to the PMHS -559 video from the UVA lateral far-side sled test S0091 (14 pulse in 90deg) at 0msec, 40msec, 80msec and 120msec.

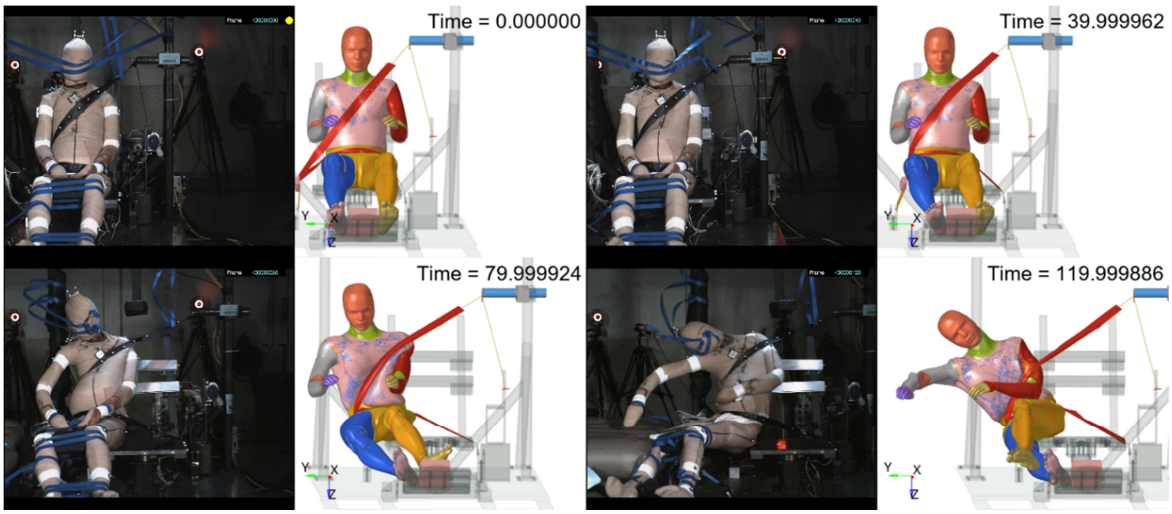

Figure 9. Snapshots of the GHBMC M50-O model v6.0 kinematics compared to the PMHS -559 test video from the UVA lateral sled test S0091 (14g pulse at 90deg) at 0msec, 40msec, 80 msec, and 120msec (Courtesy: The PMHS test data provided by UVA).

Figure 10 shows the time-histories of the responses and kinematics target relative-to-seat displacements of the GHBMC M50-O model v6.0 compared to the Vicon data of PMHS -559 in the UVA lateral far-side sled test S0091 (14g pulse in 90deg). It is seen from Figure 8 & 9 that the HBM kinematics is like the PMHS until ~80 msec. After then, the HBM has more lateral bending movement of the head/neck/torso compared to the PMHS mainly due to the seatbelt slipping down the HBM upper body after ~90msec. The difference of the body shape especially the abdomen between the PMHS -559 and the HBM is a major cause for the seatbelt loading path change. The fat abdomen of the PMHS holds the belt along the upper body longer.

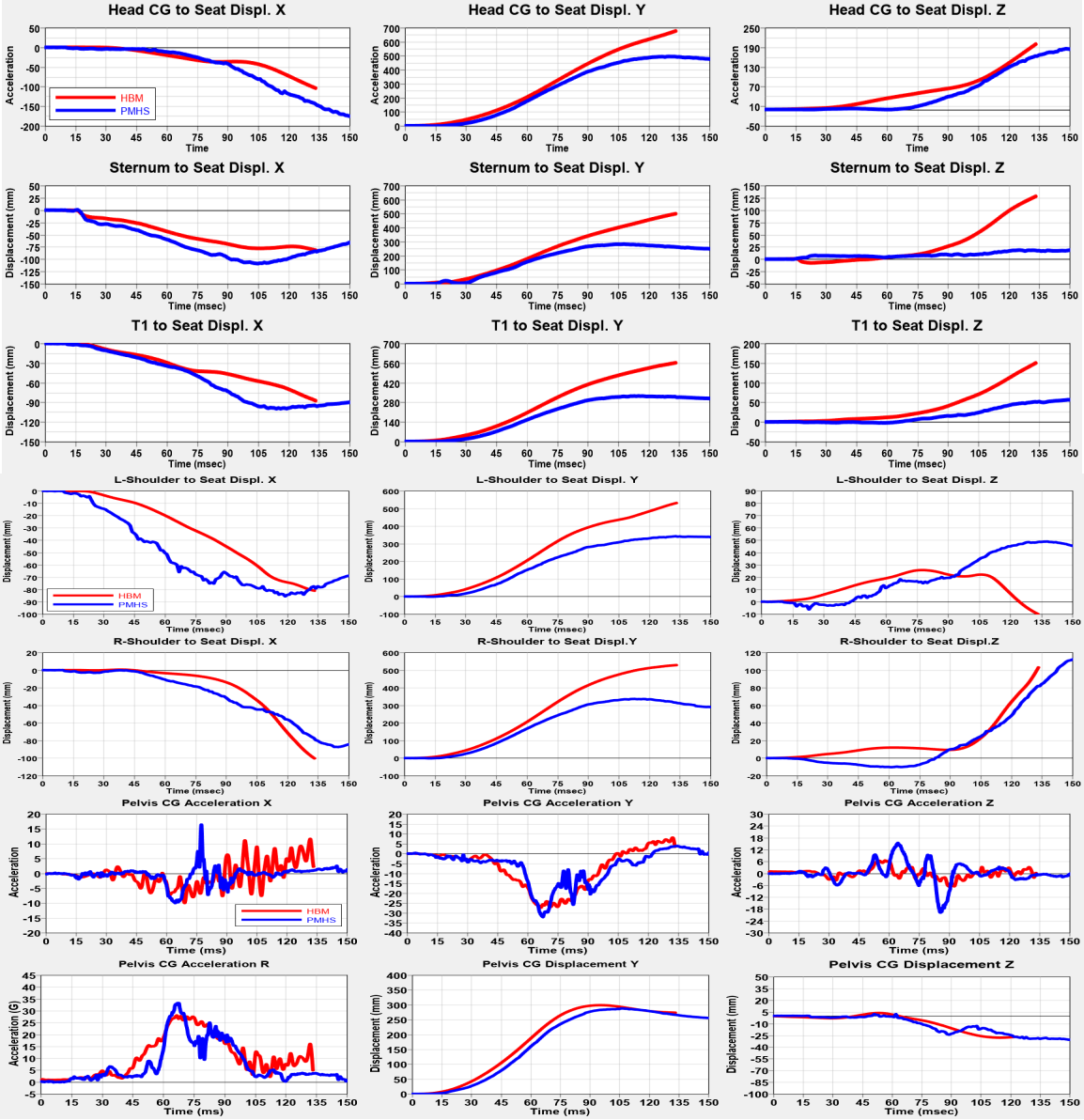

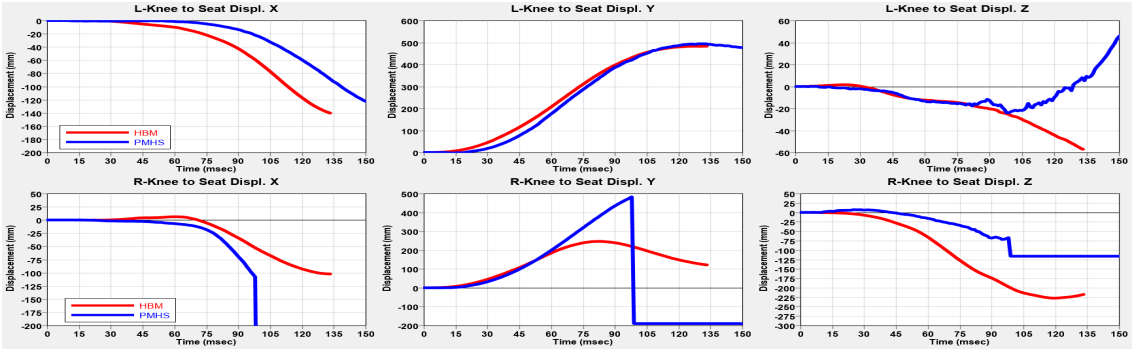

Figure 10. The time-histories of responses and kinematics target relative displacements of the GHBMC M50-O model v6.0 (Red curve) compared to the test data of PMHS -559 (Blue curve) from the UVA lateral far-side sled test S0091 (14g pulse at 90deg). (Courtesy: The PMHS test data provided by UVA).

Far-side Sled Test Occupant Simulations Results

Table B-1 in Appendix B lists the raw data of calculated responses and injury measures for all the sled simulation cases (C1 through C13) in matrix I & II with the three occupant models (GHBMC AM50-O v6.0 HBM, Humanetics WorldSid-50M model v7.6 & THOR model v1.8.1). Table B-2 in Appendix B summarizes the maximum relative-to-seat displacements of the kinematics targets of head, T1, T4, T12, pelvis, left and right shoulders and knees of those cases. Detailed data analysis results are presented in the following sub-sections.

THOR-HBM comparative analysis

Figure 11 shows snapshots of the GHBMC M50-O model v6.0 HBM kinematics at 0msec, 40msec, 80msec, and 150msec from the simulated sled test case (C2-HM135 in Table 4) with the steel seat in comparison to the paired THOR dummy case C6-TR138 (Table 4) at the 60 deg oblique sled test with 14g pulse, where the green is for the Thor dummy and the yellow for the HBM. It is seen that the Thor dummy has similar kinematics of the head/neck/torso but different lower legs movement compared to the HBM. The THOR pelvis and lower legs has much less lateral swing and upward movement than the HBM after ~80 msec.

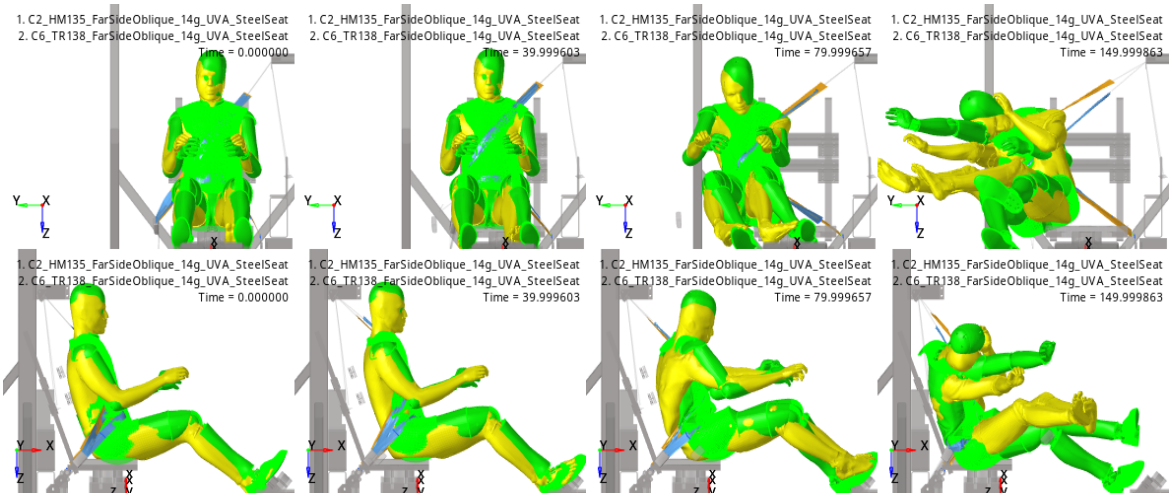

Figure 11. Snapshots of the kinematics of GHBMC M50-O model v6.0 from the simulated 14g 60 deg oblique far-side UVA sled test case C2-HM135 compared to the paired THOR dummy case C6-TR138. (Green: the Thor dummy; Yellow: the HBM). .

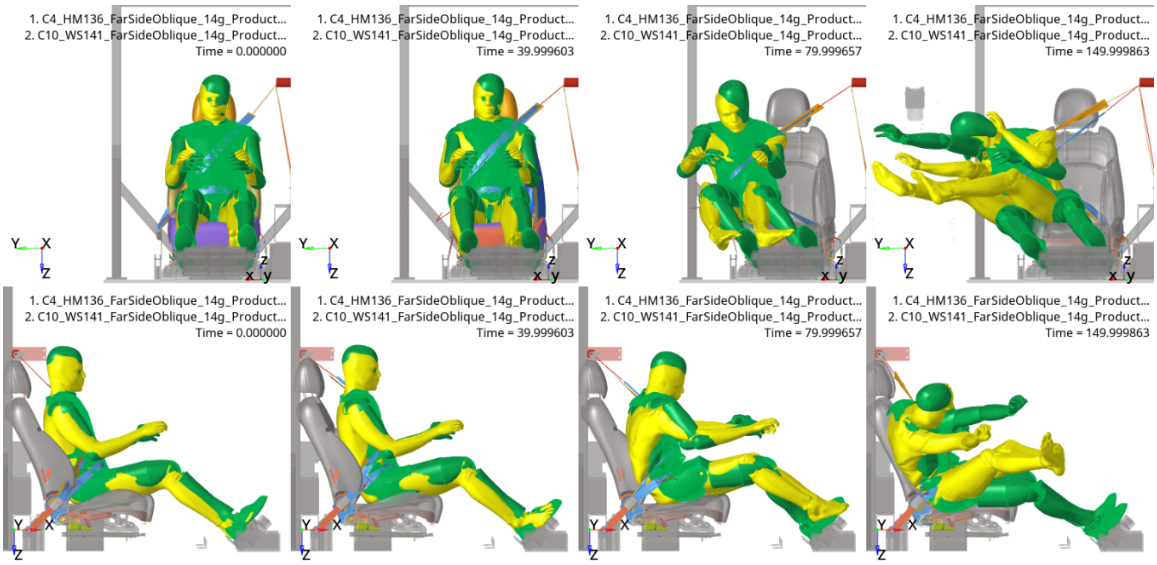

Figure 12. Snapshots of the kinematics of GHBMC M50-O model v6.0 from the simulated 14g 60 deg oblique far-side sled test with the production seat (case C4-HM136) compared to the paired THOR dummy case C7-TR139. (Green: the THOR dummy; Yellow: the HBM). .

The similar kinematics behavior of the THOR dummy is also shown in the 60 deg oblique sled test with 14g pulse with the production seat. Figure 12 shows snapshots of the GHBMC M50-O model v6.0 HBM kinematics at 0msec, 40msec, 80msec, and 150msec from the simulated sled test case C4-HM136 (Table 4) in comparison to the paired THOR dummy case C7-TR139 (Table 4).

More kinematics comparisons are made for the lateral relative-to-seat displacements of the body targets. Figure 13 compares the maximum relative-to-seat Y-displacements of the head, T1, T4, T12, pelvis, and left and right shoulders and knees between the THOR (in green) and the HBM (in yellow) for the three paired cases—C2-HM135/C6-TR138 with the UVA steel seat, C4-HM136/C7-TR139 with the production seat, and C5-HM137/C8-TR140 with the production seat and console. Under the three sled conditions, the THOR head/neck/torso moved laterally slightly more than the HBM while its lower legs lateral displacements were smaller.

Figure 13. Comparison of the maximum relative lateral Y-displacements of the head, T1, T4, T12, pelvis, and left and right shoulders and knees between the THOR and the HBM for the three paired cases—C2-HM135/C6-TR138 with the UVA steel seat, C4-HM136/C7-TR139 with the production seat, and C5-HM137/C8-TR140 with the production seat and console. (Green: the THOR dummy; Yellow: the HBM).

Figure 14 compares the normalized responses and injury measures between the GHBMC M50-O model v6.0 HBM and the THOR dummy v1.8.1 for the three THOR-HBM paired cases. Compared to the HBM, the THOR has slightly higher BrIC and acetabulum forces while the other measures are close to the HBM for all the three cases.

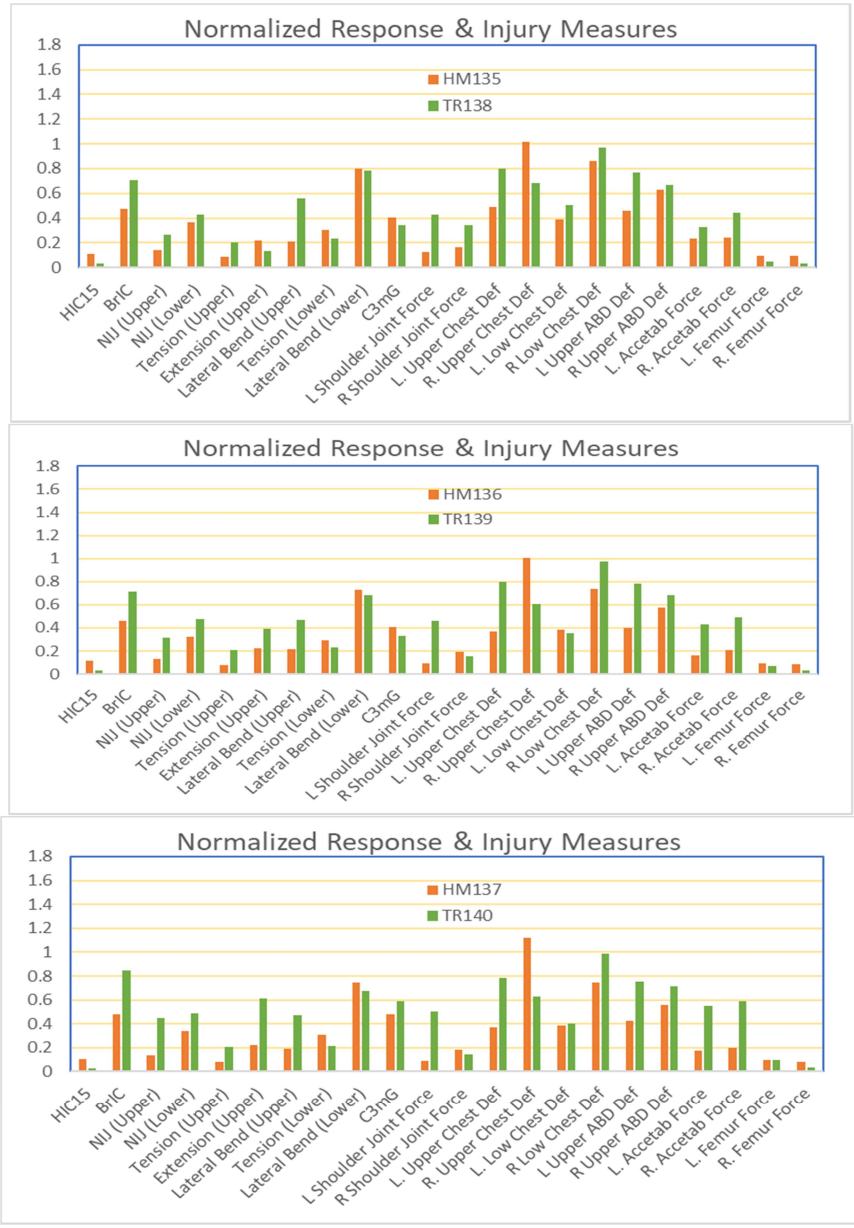

Figure 14. Comparison of the normalized responses and injury measures between the GHBMC M50-O model v6.0 and the THOR dummy model v1.8.1 for the three paired cases—C2-HM135/C6-TR138 with the UVA steel seat, C4-HM136/C7-TR139 with the production seat, and C5-HM137/C8-TR140 with the production seat and console. (Green: the THOR dummy; Yellow: the HBM).

Table 8 summarizes the calculated injury risks of the body regions of head, neck, thorax, abdomen, pelvis, and knee-thigh from the simulated far-side sled tests for the three paired THOR-HBM cases. The three THOR cases (TR138, TR139, TR140) are evaluated with the THOR model v1.8.1, and the HBM cases (HM135, HM136, HM137) are with the GHBMC M50-O model v6.0. Both the HBM and THOR models predict the highest injury risk for the chest, followed by high risks for the abdomen and pelvis regions. As the impact to the console where is at presence, the THOR model shows higher pelvis injury risk while the HBM has higher abdomen injury risk.

Table 8.
Comparison of HBM/THOR injury risks from the simulated far-side sled tests

Body Region	Measure	Risk	HM135-UVASeat HBM Injury Risk	HM136-GSeat HBM Injury Risk	HM137-GSeatCC HBM Injury Risk	TR138-UVASeat THOR Injury Risk	TR139-GSeat THOR Injury Risk	TR140-GSeatCC THOR Injury Risk
Head	HIC	AIS3+	0.0%	0.0%	0.0%	0.0%	0.0%	0.0%
	BrIC	AIS 3+	0.0%	0.0%	0.0%	14.2%	14.4%	34.0%
Neck	NIJ	AIS3+	0.5%	0.5%	0.5%	1.0%	1.3%	2.6%
Thorax	Max Thoracic rib Deflection CD	AIS3+	50.9%	49.7%	72.3%	54.0%	54.7%	56.0%
Abdomen	Max Abdomen rib Deflection ABD	AIS3+	10.0%	5.7%	40.9%	18.1%	19.2%	16.4%
Pelvis	Max. Res. Acetabulum Force	AIS 2+	2.2%	2.2%	9.0%	12.0%	23.5%	53.4%
Knee-Thigh	Fz	AIS 2+	1.0%	1.0%	1.0%	0.0%	0.0%	0.0%
Whole Body	OIM		57.4%	54.3%	85.3%	71.8%	76.4%	89.0%

WORLDSID-HBM comparative analysis

Figure 15 shows snapshots of the GHBMC M50-O model v6.0 HBM kinematics at 0msec, 40msec, 80msec, and 150msec from the simulated sled test case C2-HM135 (Table 4) in comparison to the paired WORLDSID-50M dummy case C9-WS141 (Table 4) for the 60 deg oblique UVA sled test with 14g pulse with the UVA steel seat, where the blue is for the WorldSid-50M dummy and the yellow for the human model (HBM). It is seen that the WorldSID dummy and the HBM has similar kinematics during the time up to ~70msec. After then the HBM has more lateral torso bending and lateral head/neck excursion movement than the WorldSID dummy.

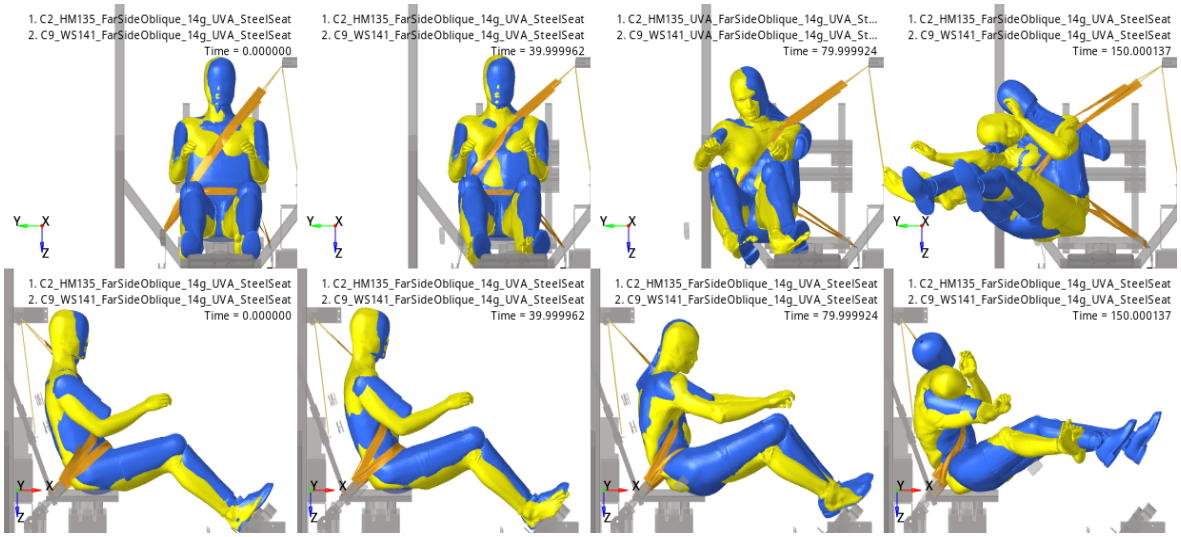

Figure 15. Snapshots of the kinematics of GHBMC M50-O model v6.0 from the simulated 14g 60deg oblique far-side steel seat sled test case C2-HM135 compared to the paired WORLDSID-50M dummy case C9-WS141. (Blue: the WorldSid-50M dummy; Yellow: the HBM).

Figure 16 shows snapshots of the GHBMC M50-O model v6.0 HBM kinematics at 0msec, 40msec, 80msec, and 150msec for the simulated sled test case C4-HM136 (Table 4) in comparison to the paired WORLDSID-50M dummy case C10-WS142 (Table 4) for the 60 deg oblique UVA sled test with 14g pulse with the production seat. The ATD-HBM kinematics differences are observed for this sled condition as well.

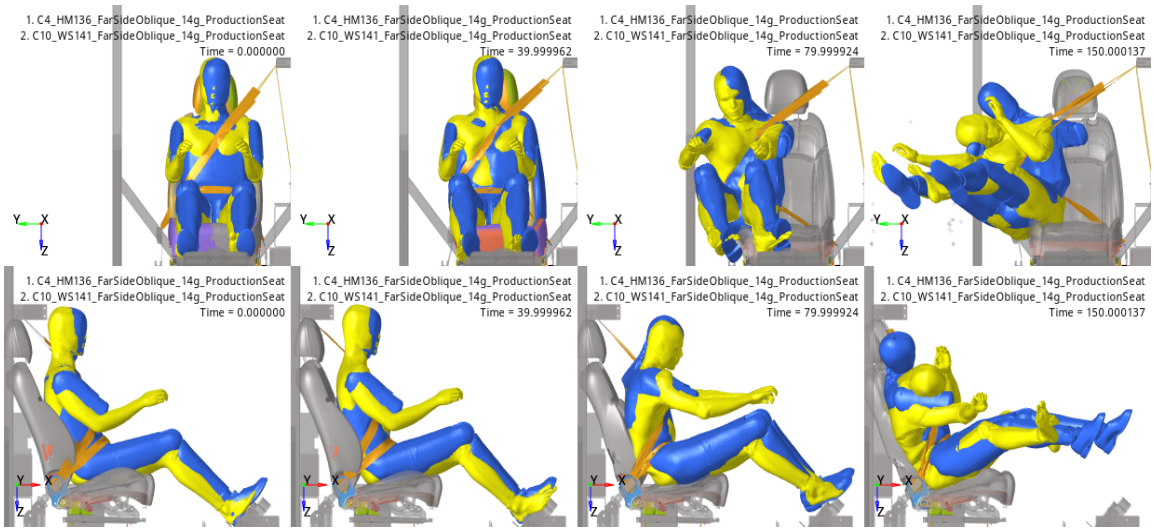

Figure 16. Snapshots of the kinematics of GHBMC M50-O model v6.0 in the simulated 14g 60deg oblique far-side production seat sled test case C4-HM136 compared to the paired WORLDSID-50M dummy case C10-WS141. (Blue: the WorldSid-50M dummy; Yellow: the HBM).

Figure 17 shows snapshots of the GHBMC M50-O model v6.0 HBM kinematics at 0msec, 40msec, 80msec, and 150msec from the simulated sled test case C5-HM137 (Table 4) in comparison to the paired WORLDSID-50M dummy case C11-WS143 (Table 4) for the 60 deg oblique UVA sled test with 14g pulse with the production seat and side console. With presence of the side console the WorldSID has more lateral bending movement but is still behind the HBM.

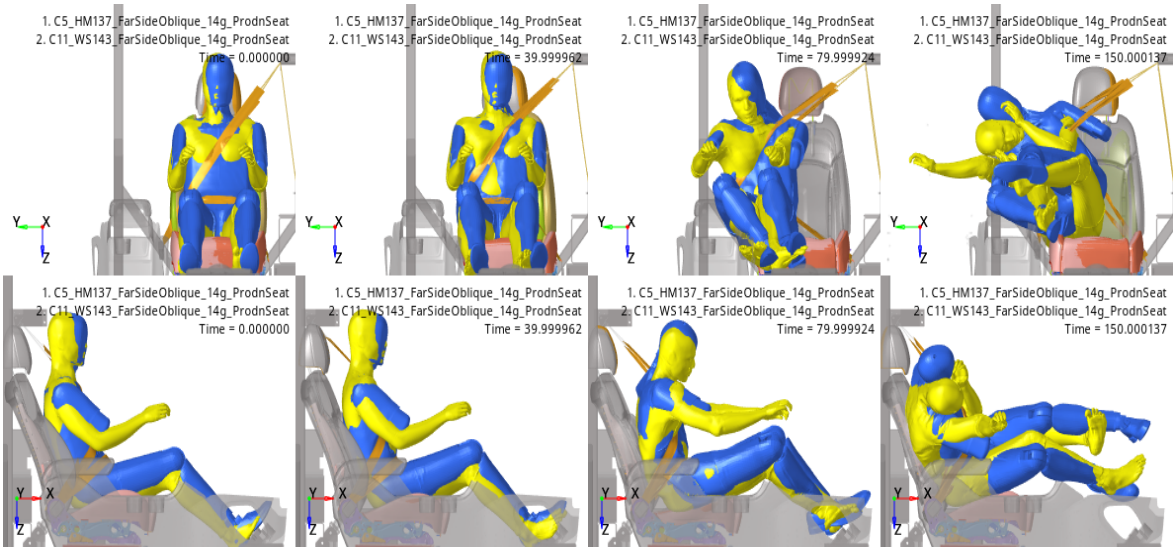

Figure 17. Snapshots of the kinematics of GHBMC M50-O model v6.0 in the simulated 14g 60deg oblique production seat/console sled test case C5-HM137 compared to the paired WORLDSID-50M dummy case C11-WS143. (Blue: the WorldSid-50M dummy; Yellow: the HBM)

Figure 18 shows snapshots of the GHBMC M50-O model v6.0 HBM kinematics at 0msec, 40msec, 80msec, and 140msec from the simulated sled test case C3-HM091 (Table 4) in comparison to the paired WORLDSID-50M dummy case C12-TR144 (Table 4) for the 90 deg lateral UVA steel sled test with the 14g pulse. Under such a lateral loading, the HBM has significantly more lateral torso bending and lateral head/neck excursion movement than the WorldSID dummy after ~70ms.

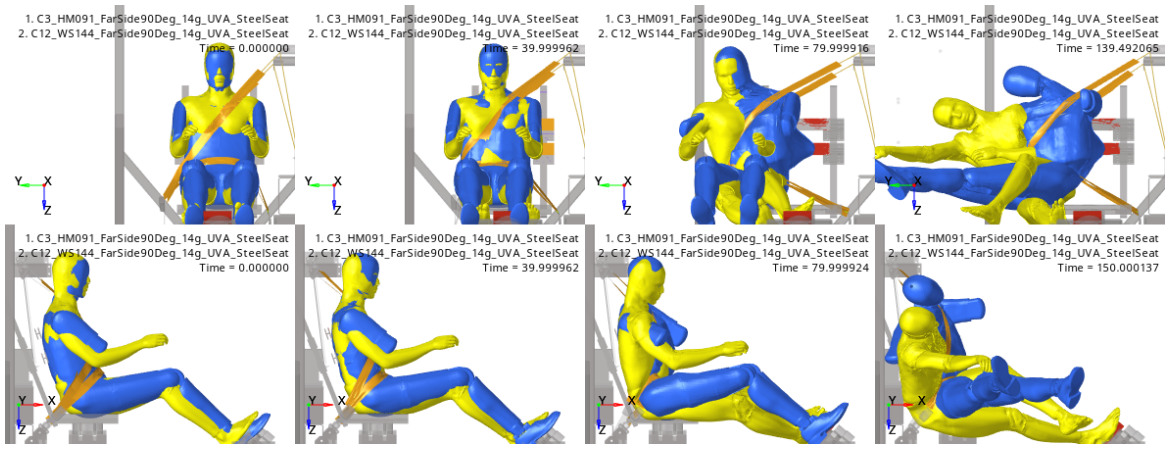

Figure 18. Snapshots of the kinematics of GHBMC M50-O model v6.0 in the simulated 14g 90deg lateral steel seat sled test case C3-HM091 compared to the paired WORLDSID-50M dummy case C12-WS144. (Blue: the WorldSid-50M dummy; Yellow: the HBM)

Figure 19 compares the maximum relative-to-seat lateral Y-displacements of the head, T1, T4, T12, pelvis, and left and right shoulders and knees between the WORLDSID and the HBM for the four paired cases (C2-HM135/C9-WS141, C4-HM136/C10-WS142, C3-HM091/C12-WS144, and C5-HM137/C11-WS143). It is seen that for the three 60 deg oblique sled test conditions (C2-C9, C4-C10, C4-C11) the maximum lateral displacements of the WORLDSID's head/neck/torso are close to the HBM, while the knees move laterally more than the HBM. For the 90deg side sled test conditions (C3-C12), however, the lateral displacements of the head/neck/torso of the WORLDSID are significantly smaller than the HBM, indicated a stiffer spine of the WORLDSID responding to the lateral loading.

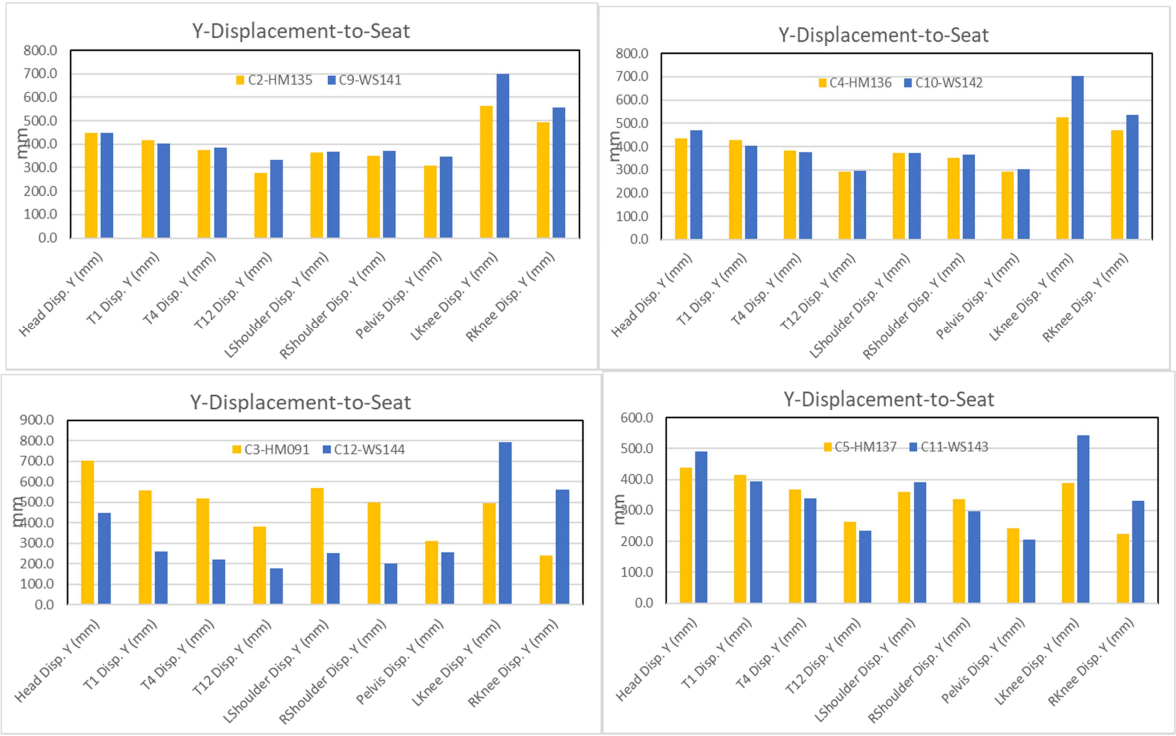

Figure 19. Comparison of the maximum relative-to-seat Y-displacements of the head, T1, T4, T12, pelvis, and left and right shoulders and knees between the THOR and the HBM of the four paired cases (HM135-WS141, HM136-WS142, HM137-WS143, HM091-WS144). (Blue: the WORLDSID dummy; Yellow: the HBM)

Figure 20 compares the normalized responses and injury measures between the GHBMC M50-O model v6.0 HBM and the WORLDSID dummy model v7.6 for the four paired cases (C2-HM135/C9-WS141, C4-HM136/C10-WS142, C3-HM091/C12-WS144, and C5-HM137/C11-WS143). It is seen that the chest/abdomen deflections of the WORLDSID are lower than the HBM for all the four simulated sled test conditions.

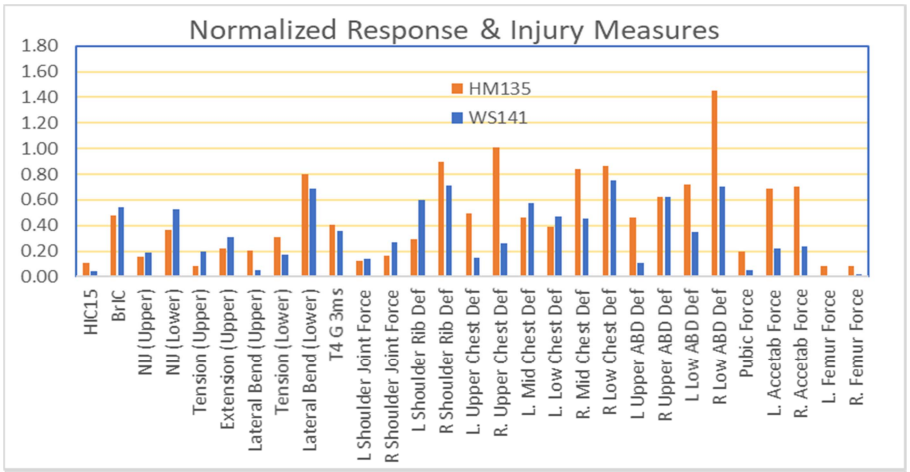

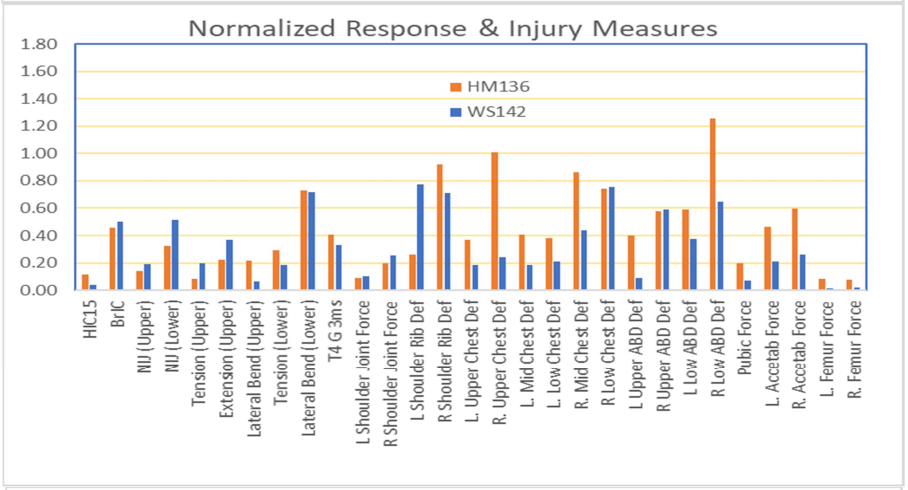

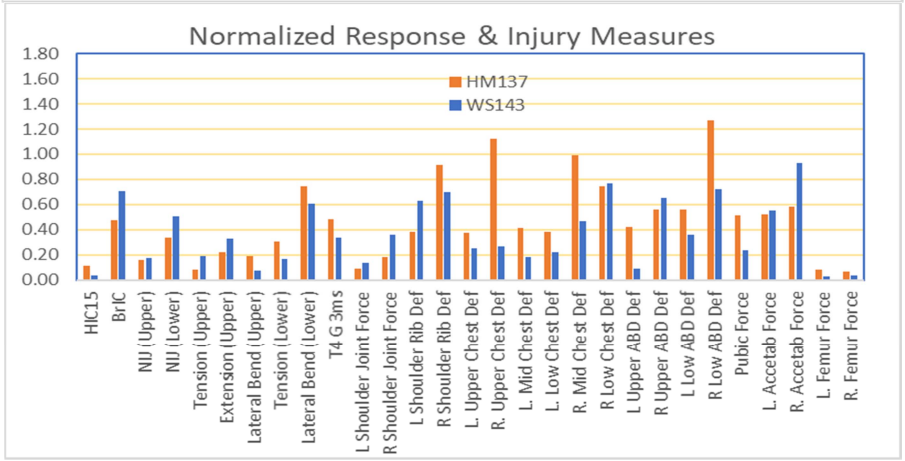

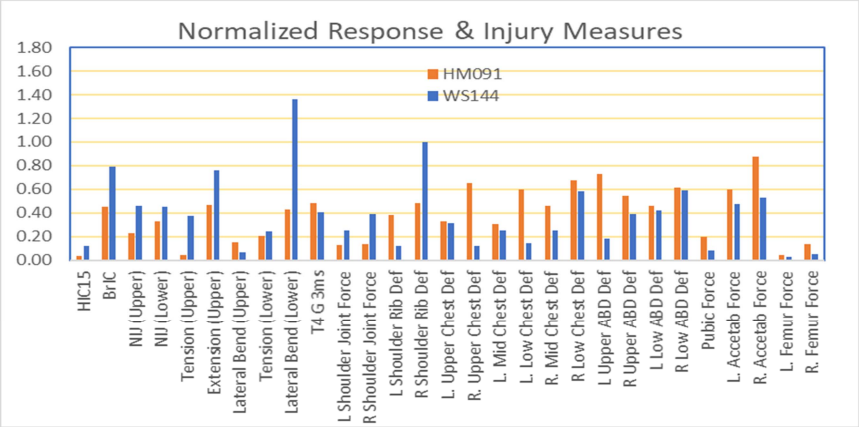

Figure 20. Comparison of the normalized responses and injury measures between the GHBMC M50-O model v6.0 and the WorldSid dummy model v7.6 for the four paired cases (C2-HM135/C9-WS141, C4-HM136/C10-WS142, C5-HM137/C11-WS143, and C3-HM091/C12-WS144). (Blue: the WORLDSID dummy; Yellow: the HBM)

Table 9 compares the injury risks of the body regions for the four HBM simulation cases (HM135, HM136, HM 137, HM091) estimated with the GHBMC M50-O model v6.0 and the four paired WORLDSID-50M cases (WS141, WS142, WS144, WS143) estimated with the WORLDSID-50M model v1.8.1.

Table 9.
Comparison of HBM/WORLDSID-50M injury risks for the simulated far-side sled tests cases

Body Region	Measure	Risk	C2-HM135 60deg UVA Seat HBM Injury Risk	C4-HM136 60deg Prod Seat HBM Injury Risk	C5-HM137 60deg Prod SeatCC HBM Injury Risk	C3-HM091 90deg UVA Seat HBM Injury Risk	C9-WS141-60deg UVA Seat WSID Injury Risk	C10-WS142-60deg Prod Seat WSID Injury Risk	C11-WS143-60deg Prod Seat-CC WSID Injury Risk	C12-WS144-90deg UVA Seat WSID Injury Risk
Head	HIC	AIS3+	0.0%	0.0%	0.0%	0.0%	0.0%	0.0%	0.0%	0.0%
	BrIC	AIS 4+	0.0%	0.0%	0.0%	0.0%	0.1%	0.0%	9.8%	18.6%
Neck	Nt	AIS3+	0.0%	0.0%	0.0%	0.0%	0.0%	0.0%	0.0%	0.1%
	NIJ	AIS3+	0.5%	0.5%	0.5%	0.7%	6.0%	6.1%	5.8%	11.3%
Thorax	Max Thoracic rib Deflection	AIS3+	50.9%	49.7%	72.3%	5.2%	8.7%	8.8%	10.4%	49.6%
Abdomen	Max Abdomen rib Deflection	AIS2+	10.0%	5.7%	40.9%	0.0%	3.2%	1.6%	3.8%	0.7%
Pelvis	Max. Pubic Force (N)	AIS2+	2.2%	2.2%	9.0%	2.2%	0.0%	0.0%	0.1%	0.0%
KTH	Fz	AIS 2+	1.0%	1.0%	1.0%	1.2%	0.7%	0.7%	0.8%	0.8%
Whole Body	OIM		57.4%	54.3%	85.3%	9.1%	17.7%	16.4%	27.4%	64.2%

Vehicle Crash Far-side Occupant Simulations Results

Table C-1 in Appendix C lists the raw data of the calculated responses and injury measures calculated with the two occupant models (GHBMC AM50-O v6.0 HBM, and WorldSid-50M model v7.6) from the paired simulation cases in matrix III (Table 6) for the vehicle pole crash test. Table C-2 in Appendix C summarizes the maximum relative displacements of the kinematics targets of head, T1, T4, T12, pelvis, left and right shoulders and knees for the two cases. Detailed data analysis results are presented in the following sub-sections.

WORLDSID-HBM comparative analysis

Figure 21 shows snapshots of the GHBMC M50-O model v6.0 HBM kinematics at 0msec, 40msec, 80msec, and 150msec for the simulated vehicle pole crash test case C14-HM146 (Table 6) in comparison to the paired WORLDSID-50M dummy case C15-WS147 (Table 6), where the blue is for the WorldSid-50M dummy and the yellow for the human model (HBM). It is seen that the occupant represented with the HBM rotates far toward the right-hand side during the crash event.

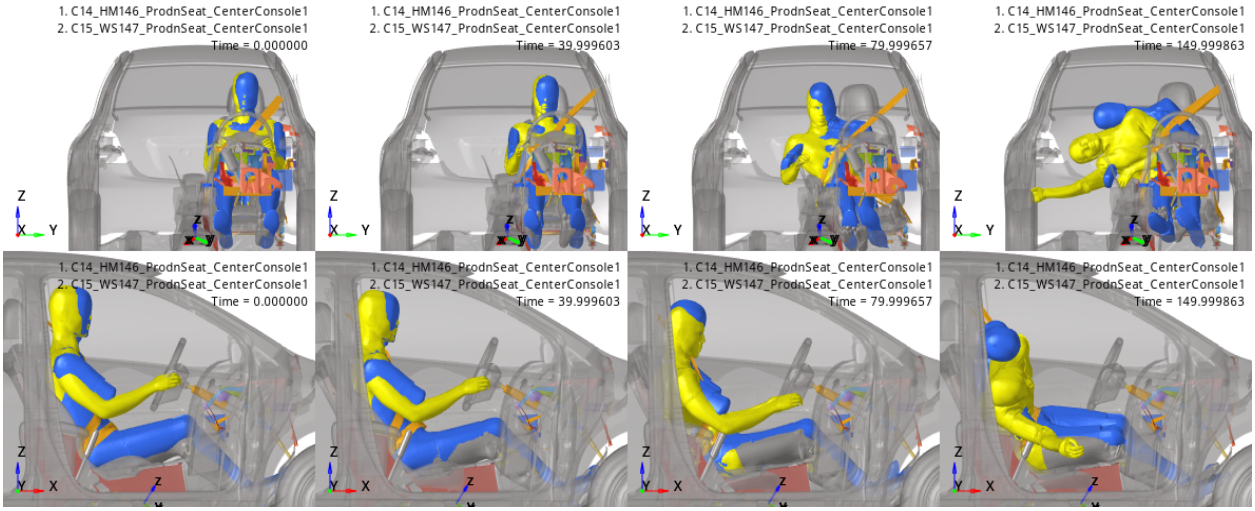

Figure 21. Snapshots of the kinematics of GHBMC M50-O model v6.0 in the simulated vehicle pole crash test case C14-HM146 in comparison to the paired WORLDSID-50M dummy case C15-WS147. (Blue: the WorldSid-50M dummy; Yellow: the HBM).

The WORLDSID-50M dummy model behaves similar kinematics like that from the lateral sled case C3-HM091 shown in Figure 19—the lateral excursion of the head/neck, shoulders and torso are less than the HBM for this vehicle crash case. Figure 22 further shows that the maximum relative displacement-Y of the head, T1, T4, T12, pelvis, and left and right shoulders and knees of the WORLDSID are all smaller than the HBM under the same FMVSS 214 subject vehicle pole crash condition.

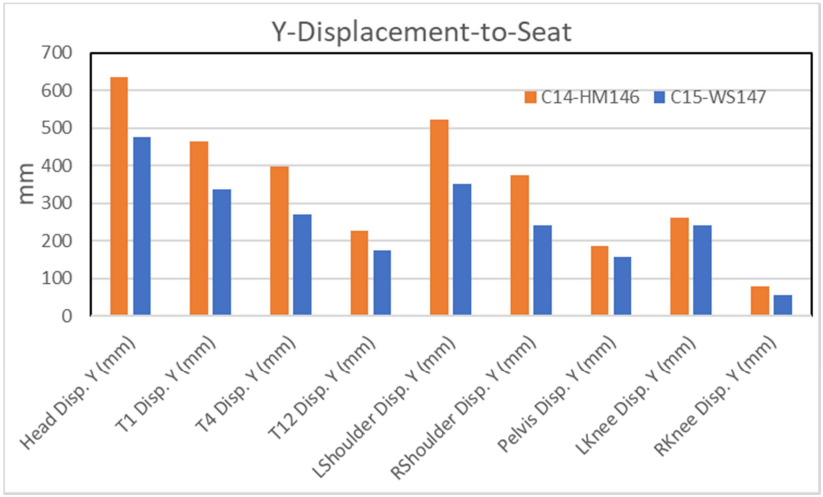

Figure 22. Comparison of the maximum relative lateral Y-displacements of the head, T1, T4, T12, pelvis, and left and right shoulders and knees between the WORLDSID and the HBM of the paired case (C14-HM146/C15-WS147) for the FMVSS 214 compact vehicle pole crash. (Blue: the WORLDSID dummy; Yellow: the HBM)

Figure 23 compares the normalized response and injury measures between the HBM and the WORLDSID-50M from the vehicle pole crash test simulations. The chest deflections from the WORLDSID-50M model are lower than that predicted with the HBM.

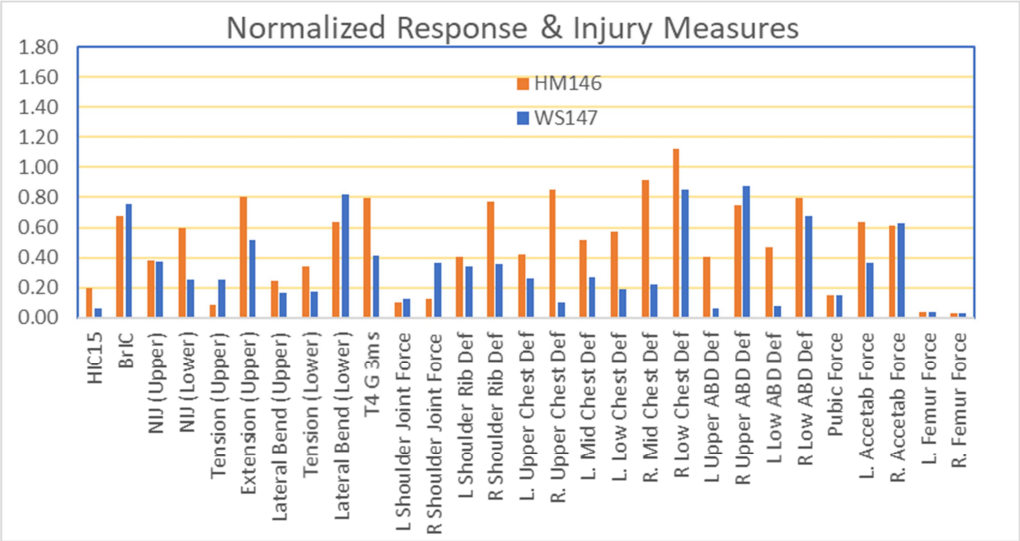

Figure 23. Comparison of the normalized response and injury measures between the AM50-O v6.0 HBM case C14-HM146 and the WorldSID-50M model v7.6 case C15-WS147 from the vehicle pole crash simulations. (Blue: the WORLDSID dummy; Yellow: the HBM)

Table 10 compares the body regions injury risks estimated with the GHBMC M50-O model v6.0 from the HBM vehicle crash simulation cases HM146 and the WORLDSID-50M model v7.6 from the paired WORLDSID-50M case WS147. The injury risks for all the other body regions are similar between the WorldSID and the HBM except for the chest where the WorldSID's estimated risk is lower than the HBM due to less chest deflections.

Table 10.
Comparison of HBM/WORLDSID-50M injury risks for the from the vehicle pole crash cases

Body Region	Measure	Risk	HM146- from Vehicle Pole Crash HBM Injury Risk	WS1147- from Vehicle Pole Crash WORLDSID Injury Risk
Head	HIC	AIS3+	0.1%	0.0%
	BrIC	AIS 4+	10.4%	14.9%
Neck	Nt	AIS3+	0.0%	0.0%
	NIJ	AIS3+	1.5%	9.3%
Thorax	Max Thoracic rib Deflection	AIS3+	73.4%	20.4%
Abdomen	Max Abdomen rib Deflection	AIS2+	12.2%	19.7%
Pelvis	Max. Pubic Force (N)	AIS2+	1.8%	0.0%
KTH	Fz	AIS 2+	0.8%	0.8%
Whole Body	OIM		80.0%	51.1%

DISCUSSIONS

Model Predicted Injury Risks Verification

Table 12 compares the model predicted injury risks with the PMHS post-test Autopsy examination results from the UVA far-side tests. For the PMHS 602 oblique sled test conditions, both the HBM and THOR model predicted high chest injury risk which is in line with the post-test observation. The WorldSID dummy model

underestimates the chest injury risk for this PMHS due to the lower chest deflections. For the PMHS 559 test condition, the WorldSID predicted high chest injury risk which is in line with the test outcomes while the HBM's prediction underestimates the risk. The cause is that the seatbelt slipping down the HBM body after ~80msec which lower the chest loading force for the HBM correlation case C3-HM091 as shown in Figure 9. This phenomenon may be occupant body shape dependent. This issue should be further investigated. The HBM correlation for the lateral sled case C3-HM09 will be improved.

Table 12.
Verification of HBM predicted injury risks with the Autopsy examination reported results

PMHS #	Body Region	Injury	AIS Code 2005 (1998 where different)	HBM Predicted Injury risk	WorldSID Predicted Injury risk	THOR Predicted Injury risk
PMHS 602	Thorax	Fractures of 5 Left ribs (L4, L5, L6, L7, L9) and 4 right ribs (R2, R3, R5, R6) (without flail)	450203.3 (450230.3)	AIS 3+ risk 57.4%	AIS 3+ risk 17.7%	AIS 3+ risk 54.3%
	Thorax	Sternum fracture* (note that this fracture involved one of the sternum instrument mount holes, thus may be artifactual)	450804.2			
	Lumbar Spine	Transverse process fracture, L2 left side	650620.2	NA	NA	NA
PMHS 559	Thoracic Spine	Vertebral body fracture (NFS), T10	650430.2	AIS 3+ risk 9.1%	AIS 3+ risk 64.2%	NA
	Thorax	Sternum fracture	450804.2			
	Thorax	Bilateral flail chest (by definition - ≥3 ribs fractured in more than one location, bilaterally)	450214.5 (450266.5)			

Kinematics & Response Differences between the HBM and the WorldSID Model

From the vehicle pole crash simulations, difference of the lateral movements of the WorldSID model and the HBM is observed during the vehicle crash event. The kinematics comparison is shown in Figure 21. Figure 22 indicates the less lateral displacements of the dummy targets than the HBM's. Figure 24 compares the external forces to the occupant between the HBM and the WorldSID-50M during the period of 130 msec. It is observed that the HBM has experienced larger contact force by the center console in the longer interaction duration even though the other external forces to the HBM from the seatbelt and seat are larger than the ATD. The larger console contact force causes much larger chest and abdominal deflections to the HBM. The WorldSID dummy model showed stiffer torso bending and earlier rebounce of the body away from the center console.

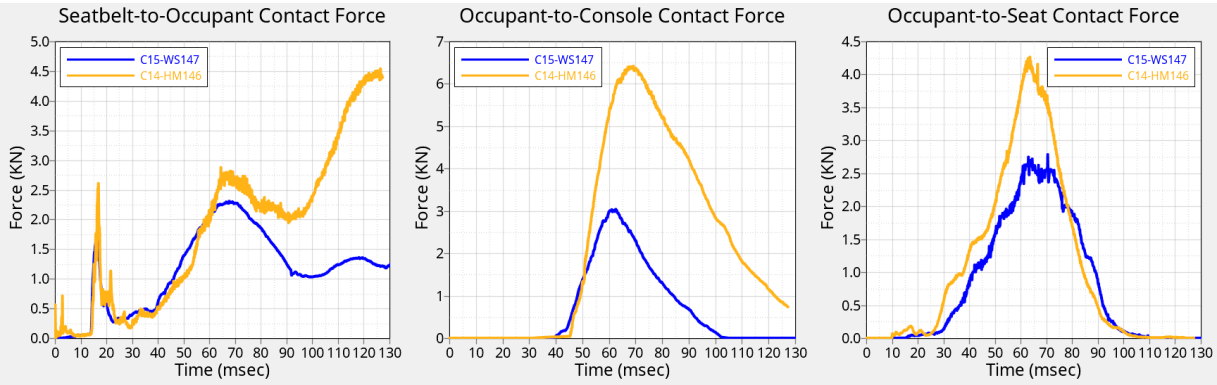

Figure 24. Comparison of the external forces to the occupant between the HBM case C14-HM146 and the WorldSID-50M case C15-WS147 from the vehicle pole crash simulations. (Blue: the WORLDSID dummy; Yellow: the HBM)

Kinematics & Response Differences between the HBM and the THOR Model

The THOR dummy model has the kinematics and response similar to the HBM from the simulated oblique sled tests, as shown in Figures 11 - 14. Major differences observed are the kinematics of the lower extremities. Compared to the HBM, the THOR lower legs have less lateral swing and upward movement in the oblique far-side

sled tests. Figure 25 shows comparison of the external forces to the occupant between the HBM and the WorldSID-50M during the period of 150 msec in the simulated far-side sled test S135 (14g pulse in 60deg), including the total seatbelt forces to the occcupant, and the forces from the foot plate to the left and right foot. Although all the relevant contact parameters such as the friction coefficients and penalty factors are defined same for those external contacts, the contact forces for the HBM and the WorldSID are still different. Compared to the HBM, the THOR dummy model has the longer duration in the right foot contact force and higher peak force to the left foot, which is mainly due to insufficient lift up motion of the THOR legs as compared to the observed from PMHS or the HBM in the test. This could indicate poor biofidelity of the THOR pelvis responding to the lateral inertia loads.

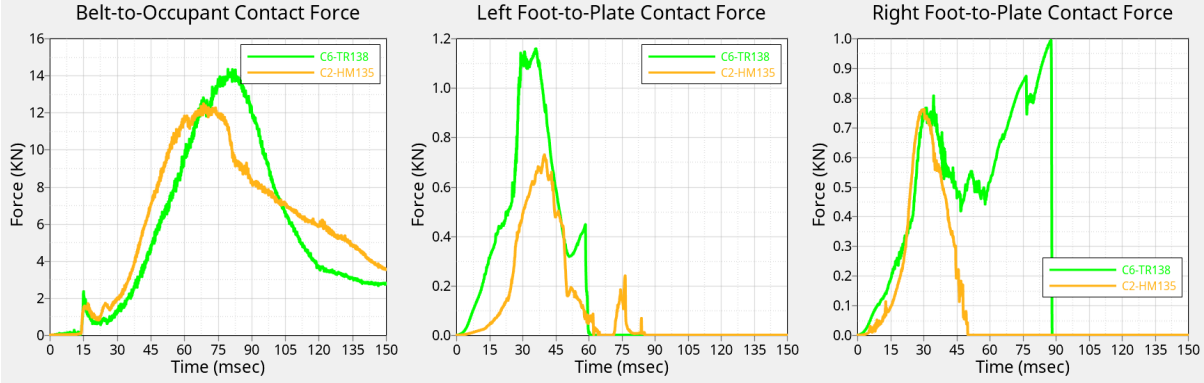

Figure 25. Comparison of the external forces to the occupant between the HBM case C2-HM135 and the THOR case C6-TR138 from the simulated far-side sled test S135 (14g pulse at 60deg). (Yellow: the HBM; Green: the THOR)

Limitations of this Study

This study generates a large set of data from the thirteen sled test simulations and two vehicle crash occupant simulations with the HBM (the GHBMC AM50-O model v6.0), and the two ATD models (Humanetics WorldSID model v7.6 & THOR model v1.8.1). Although the two ATD models have been validated at some extent with other component and sled system level tests, the current simulated results with the ATDs are not validated directly with the physical far-side sled tests. This could be the next step for this study.

In this study, the results of the occupant body region injury risks predicted by the HBM and the ATDs show some inconsistence from case to case due to the differences of the kinematics and responses under the far-side crash loading conditions. As the kinematics and responses are mainly affected by the regular/non-regular restraints (seatbelt, seats, consoles, etc.) under the defined far-side crash mode, a larger set of restraint and environment component variants are not studied yet. More analysis and experimental verification for the restraint influence individually and comparably for the HBM and ATDs are helpful for identifying biofidelic deficiencies of the ATDs and improving the restraint performance as well. In addition, the injury risk functions for each of the mid-sized male occupant models used in this study could be further evaluated and improved.

CONCLUSIONS

The latest GHBMC 50th percentile male occupant model version v6.0 is validated with the PMHS tests under the two oblique (60deg) far-side sled tests varying the pulse severities from 6.6g to 14g. The HBM predicted high injury risks for the thorax under such test conditions are in line with the post-test PMHS injury observations.

For the 90deg lateral sled test under the 14g pulse, the HBM demonstrates reasonably biofidelic kinematic responses compared to the PMHS, although the case correlation can be further improved. It seems that for such a crash mode, the occupant body shape seems to have more influence on the seatbelt restraints which needs to be investigated.

The Humanetics mid-sized male THOR dummy v1.8.1 has similar head/neck/torso kinematic responses compared to the HBM in the oblique (60deg) far-side sled test condition. The swing and upward movements of the lower extremities are shown lagging behind the HBM from the simulated oblique far-side sled test, indicating poor biofidelity of the THOR pelvis and lower leg body regions responding to the lateral inertia loads.

The Humanetics mid-sized male WorldSID-50M model v7.6 has similar whole-body kinematics and responses to the HBM responding to the oblique far-side crashes. Responding to the lateral far-side loadings, the model has less body bending and thoracic rib deformations compared to the HBM, indicating a stiffer spine and thoracic ribcage.

ACKNOWLEDGEMENTS

Thanks for Jason Kerrigan, Richard Kent, Jason Forman at University of Virginia who provided the PMHS data for the human model case correlation. And thanks for Scott Gayzik's team at Wake Forest University School of Medicine who provided the GHBMC human body model for this study. And thanks are given to Sungwoo Lee who helped the FE work for the subject vehicle model building and some case analysis.

REFERENCES

[1] FORMAN, J., Lopez-Valdes, F., et al. 2013. "Occupant kinematics and shoulder belt retention in far-side lateral and oblique collisions: a parametric study." Stapp Car Crash Journal, 57: pp.343–85.

[2] Diggers, K., Dalmotas, D., 2001. "Injuries to restrained Occupants in Far-side Crashes." In Proceedings of the 17th International Technical Conference on the Enhanced Safety of Vehicles, Amsterdam, 17-0351.

[3] Yoganandan, N., Pintar, F. A., Gennarelli, T. A., Maltese, M. R. 2000. "Patterns of abdominal injuries in frontal and side impacts." Annual Proceedings of the Association for the Advancement of Automotive Medicine, 44: pp.17–36.

[4] Gabler, H. C., Fitzharris, M., Scully, J., Fildes, B. N. 2005. "Far side impact injury risk for belted occupants in Australia and the United States. Proceedings of the 19th International Technical Conference on the Enhanced Safety of Vehicles, Washington D.C., 05-0420.

[5] Bahous, G., Murakhovskiy, D., Digges, K., Rist, H., Wiik, R. 2015. "Opportunities for reducing far-side casualties." Proceedings of the 24th International Technical Conference on the Enhanced Safety of Vehicles, Gothenburg, Sweden, 15-0444.

[6] Hosteler, Z. S., Fang, C. H., Barnard, R., Jones, D. A., Davis, M. L., Weave, A. A. 2021. "Injury Risk Curves in Far-side Lateral Motor Vehicle Crashes by AIS level, Body Region and Injury Code", in Traffic Injury Prevention, v21: pp 112-117.

[7] Euro NCAP, "Far Side Occupant Test & Assessment Procedure – Implementation 2023." 2022. in European New Car Assessment Programme version 2.3, 14th November 2022.

[8] Pintar, F. A., Yoganandan, N., et al. (2007). "Comparison of PMHS, WorldSID, and THOR-NT responses in simulated far side impact." Stapp Car Crash Journal, 51: pp. 313–360.

[9] Parent, D., Craig, M., Moorhouse, K. (2017). "Biofidelity Evaluation of the THOR and Hybrid III 50th Percentile Male Frontal Impact Anthropomorphic Test Devices". Stapp Car Crash Journal, 61: pp. 227-276.

[10] Rhule, H., Moorhouse, K., Donnelly, B., Stricklin, J. 2009. "Comparison of WorldSid and ES-2re Biofidelity Using an Updated Biofidelity Ranking System". In Proceedings of the 21st International Technical Conference on the Enhanced Safety of Vehicles, Stuttgart, Germany, 09-0562.

[11] Katagiri, M., Zhao, J., Kerrigan, J., Kent, R., Forman, J.. 2016. "Comparison of Whole-Body Kinematic Behavior of the GHBMC Occupant Model to PMHS in Far-Side Sled Tests." IRCOBI Conference 2016, IRC-16-88.

[12] Eppinger, R., et al., 1999, "Development of Improved Injury Criteria for the Assessment of Advanced Automotive Restraint Systems - II", NHTSA

[13] Eppinger, R., et al., 2000, "Supplement: Development of Improved Injury Criteria for the Assessment of Advanced Automotive Restraint Systems - II", NHTSA.

[14] Takhounts, E., Craig, JC., Moorhouse, K., and McFadden, J. 2013. "Development of Brain injury Criteria (BrIC)", Stapp Car Crash Journal Vol 57: 343-266.
[15] Laituri, T., et al., 2005, "Derivation and Evaluation of a Provisional, Age-Dependent, AIS3+ Thoracic Risk Curve for Belted Adults in Frontal Impacts", SAE World Congress, 2005-01-0297.
[16] Rouhana, S. W., El-Jawahri, R. E., Laituri. T.R., 2010. "Biomechanical Considerations for Abdominal Loading by Seat Belt Pretensioners", Stapp Car Crash Journal, Vol 54: pp. 381-406.
[17] Leport, T., Baudrit, P., Trosseille, X., Petit, P., Palisson, A., Vallancien, G., 2007. "Assessment of the Pubic Force as a Pelvic Injury Criterion in Side Impact". Stapp Car Crash Journal, Vol 51: pp. 467-488.
[18] Kuppa, S., et al., 2001, "Lowe Extremity Injuries and Associated Injury Criteria", 24th ESV Conference, Paper No. 457.
[19] Petitjean, A., Trosseille, X., Praxl, N., Hynd, D., Irwin, A. 2012. "Injury Risk Curves for the WorldSID 50th Male Dummy", Stapp Car Crash Journal 56: 323-347.
[20] Craig, M., Parent, D., Lee, E., Rudd, R., Takhounts, E., Hasija, V., 2020. "Injury Criteria for the THOR 50th Male ATD". from ISO/TR 19222:2021(en) https://www.iso.org/obp/ui/#iso:std:iso:tr:19222:ed-1:v1:en.

Appendix-A: Injury Risk Functions for the HBM and ATDs

The risk injury functions for the body regions and the whole body of the HBM, THOR dummy and WORLDSID-50M dummy were summarized in Table A-1, A-2 & A-3 below.

Table A-1.
The injury risk functions for the 50th%ile male HBM

Body Region	Injury Measure	Function	Reference
Head	HIC	$P(AIS\,3+) = \emptyset\left[\frac{\ln(HIC) - 7.45231}{0.73998}\right]$	[13]
	BrIC	$P(AIS\,3+) = 1 - e^{-\left(\frac{BrIC-0.523}{0.531}\right)^{1.8}}$	[14]
Neck	Max. Upper Neck Tension, Nt (KN)	$P(AIS\,3+) = \frac{1}{1+e^{(10.9745-2.375*Nt\ or\ Nc)}}$	[13]
	NIJ	$P(AIS\,3+) = \frac{1}{1+e^{(6.047-5.44*NIJ)}}$	[20]
Thorax	Max Thoracic rib Deflection DC (mm)	$P(AIS\,3+) = \frac{1}{1+e^{(12.597-0.05861*65-26.90118*CD/210)}}$	[15]
Abdomen	Max Abdomen Vmax*Cmax (1/Sec)	$P(AIS\,2+) = \frac{1}{1+e^{(8.07533-2.77263*Vmax*Cmax)}}$	[16]
Pelvis	Max. Pubic Force, Fp (KN)	$P(AIS\,2+) = \frac{1}{1+e^{(4.70-1.5*Fp)}}$	[17]
Thigh/Knee	Max. Femur Force, Fz (KN)	$P(AIS\,2+) = \frac{1}{1+e^{(4.9795-0.326*Fz)}}$	[18]

Table A-2.
The injury risk functions for the WorldSID-50M dummy

Body Region	Injury Measure	Function	Reference
Head	HIC	$P(AIS\,3+) = \emptyset\left[\frac{\ln(HIC) - 7.45231}{0.73998}\right]$	[13]
	BrIC	$P(AIS\,3+) = 1 - e^{-\left(\frac{BrIC-0.523}{0.531}\right)^{1.8}}$	[14]
Neck	NIJ	$P(AIS\,3+) = \frac{1}{1+e^{(3.227-1.969*NIJ)}}$	[12]
Shoulder	Shoulder Rib Force, Fs (N)	$P(AIS\,3+) = 1 - e^{-\left(\frac{Fs}{2379.584}\right)^{7.409474}}$	[19]
Thorax	Max Thoracic rib Deflection CD (mm)	$P(AIS\,3+) = \frac{1}{1+e^{(3.693638-LN(CD)/0.123132)}}$	[19]
Abdomen	Max Abdomen Deflection ABD (mm)	$P(AIS\,3+) = 1 - e^{-\left(\frac{ABD}{52.3975}\right)^{8.611282}}$	[19]
Pelvis	Max. Pubic Force, Fp (N)	$P(AIS\,3+) = 1 - e^{-\left(\frac{Fp}{2456.761}\right)^{4.599182}}$	[19]
Thigh/Knee	Max. Femur Force, Fz (KN)	$P(AIS\,2+) = \frac{1}{1+e^{(4.9795-0.326*Fz)}}$	[18]

Table A-3.
The injury risk functions for the THOR dummy

Body Region	Injury Measure	Function	Reference
Head	HIC	$P(AIS\ 3+) = \emptyset\left[\frac{\ln(HIC) - 7.45231}{0.73998}\right]$	[13]
	BrIC	$P(AIS\ 3+) = 1 - e^{-\left(\frac{BrIC-0.523}{0.531}\right)^{1.8}}$	[14]
Neck	NIJ	$P(AIS\ 3+) = \frac{1}{1+e^{(6.047-5.44*NIJ)}}$	[20]
Thorax	Max Thoracic rib Deflection DC (mm)	$P(AIS\ 3+) = 1 - e^{-\left(\frac{CD}{58.183}\right)^{2.977}}$	[20]
Abdomen	Max Abdomen Deflection DC (mm)	$P(AIS\ 3+) = 1 - e^{-\left(\frac{ABD}{106.222}\right)^{4.3127}}$	[20]
Pelvis	Max. Pubic Force, Fp (KN)	$P(AIS\ 2+) = \emptyset\left[\frac{\ln(1.429 * F) - 1.6058}{0.2339}\right]$	[20]
Thigh/Knee	Max. Femur Force, Fz (KN)	$P(AIS\ 2+) = \emptyset\left[\frac{\ln(1.229 * FLC) - 2.62}{0.3014}\right]$	[20]

Appendix-B: The Far-side Sled Test Simulation Matrix I & II Results

Table B-1.
Responses and injury measures of the occupant models (GHBMC AM50-O v6.0 HBM, WorldSid-50M model v7.6 & THOR model v1.8.1) of the sled simulation cases in matrix I & II

Body Region	***Injury Measure***	C1	C2	C3	C4	C5	C6	C7	C8	C9	C10	C11	C12	C13
		HM 134	HM 135	HM 091	HM 136	HM 137	TR 138	TR 139	TR 140	WS 141	WS 142	WS 143	WS 144	WS 145
Head	***HIC15***	2.95	85.48	26.11	91.13	87.22	26.1	23.4	21.7	33.69	31.50	28.14	97.4	23.7
	BrIC	0.23	0.48	0.46	0.46	0.48	0.71	0.71	0.85	0.54	0.50	0.71	0.79	0.65
Neck	***NIJ (Upper)***	0.29	0.14	0.20	0.13	0.14	0.26	0.32	0.45	0.24	0.25	0.22	0.59	0.38
	NIJ (Lower)	0.31	0.36	0.33	0.32	0.34	0.64	0.72	0.73	0.79	0.77	0.75	0.68	0.85
	Tension (Upper)	0.08	0.36	0.19	0.33	0.34	0.84	0.86	0.87	0.84	0.82	0.79	1.57	0.82
	Extension (Upper)	2.98	5.53	11.72	5.55	5.52	4.58	13.72	21.49	10.88	12.79	11.43	26.59	14.21
	Lateral Bend (Upper)	10.67	20.78	14.88	21.57	19.17	84.33	70.72	70.46	7.38	9.79	10.67	10.32	15.14
	Tension (Lower)	0.49	1.28	0.84	1.22	1.29	0.98	0.96	0.90	0.73	0.76	0.70	1.01	0.60
	Extension (Lower)	36.27	79.78	43.19	73.25	74.25	7.85	9.85	25.03	103.62	107.34	91.20	204.30	89.22
	Lateral Bend (Lower)	20.00	24.18	28.89	24.34	28.87	118.0	101.9	101.1	21.64	19.81	20.01	24.36	23.51
Thorax	***T4 G 3ms***	0.18	0.25	0.26	0.18	0.18	20.53	19.70	35.20	0.31	0.22	0.31	0.57	0.49
	L Shoulder Joint Force	0.10	0.34	0.28	0.39	0.36	1.07	1.15	1.26	0.61	0.57	0.81	0.88	1.03
	R Shoulder Joint Force	12.83	20.01	26.24	17.85	26.12	0.86	0.39	0.36	23.99	30.9	25.27	4.79	29.99
	L Shoulder Rib Def	39.58	60.80	33.00	62.60	62.04	--	--	--	28.46	28.4	27.97	40.1	14.35
	R Shoulder Rib Def	16.98	33.46	22.08	24.97	25.29	--	--	--	5.85	7.48	10.10	12.4	17.43
	L. Upper Chest Def	30.19	68.87	44.54	68.50	76.07	43.76	43.84	43.18	10.30	9.61	10.60	4.81	3.86
	R. Upper Chest Def	23.38	31.25	20.96	27.59	28.04	37.51	33.21	34.51	22.90	7.37	7.40	10.0	9.10
	L. Mid Chest Def	22.94	26.44	40.41	26.02	26.17	--	--	--	18.72	8.37	8.82	5.80	5.76
	L. Low Chest Def	23.83	57.14	31.09	58.82	67.27	27.88	19.64	21.94	18.04	17.4	18.61	10.1	9.98

	R. Mid Chest Def	26.28	58.78	45.86	50.27	50.65	--	--	--	30.10	30.2	30.83	23.2	26.09
	R Low Chest Def	20.89	34.46	54.56	29.89	31.71	53.43	53.79	54.47	5.60	4.48	4.61	9.19	9.99
Abdomen	***L Upper ABD Def***	21.91	46.98	40.82	43.10	42.08	73.06	74.28	71.29	31.03	29.60	32.61	19.30	26.63
	R Upper ABD Def	28.30	53.91	34.49	44.27	41.95	63.11	65.04	67.61	17.66	18.84	18.03	20.98	23.50
	L Low ABD Def	47.18	109.00	46.13	94.20	94.94	--	--	--	35.26	32.45	35.92	29.50	37.84
	R Low ABD Def	0.27	0.54	1.08	0.38	0.43	--	--	--	33.69	31.50	28.14	97.35	23.72
	L Upper ABD Vmax*Cmax	0.17	0.42	0.73	0.35	0.33	--	--	--	--	--	--	--	--
	R Upper ABD Vmax*Cmax	0.27	0.65	0.53	0.49	0.51	--	--	--	--	--	--	--	--
	L Low ABD Vmax*Cmax	0.70	2.12	0.97	1.90	2.78	--	--	--	--	--	--	--	--
	R Low ABD Vmax*Cmax	0.20	0.60	0.62	0.61	1.59	--	--	--	--	--	--	--	--
Pelvis	***Pubic Force***	1.15	2.36	2.07	1.60	1.79	0.00	0.00	0.00	0.17	0.56	0.20	0.09	0.17
	L. Acetabulum Force	1.03	2.42	3.03	2.05	2.01	1.94	2.58	3.28	0.84	2.19	1.89	1.03	0.84
	R. Acetabulum Force	0.35	1.16	0.58	1.14	1.18	2.65	2.94	3.56	1.03	3.73	2.11	1.81	1.03
KTH	***L. Femur Force***	0.43	1.12	1.87	1.06	0.94	0.47	0.73	0.98	0.12	0.26	0.31	0.28	0.12
	R. Femur Force	2.95	85.48	26.11	91.13	87.22	0.33	0.35	0.38	0.19	0.37	0.52	0.36	0.19

Table B-2.
Kinematics target relative displacements of the occupant models (GHBMC AM50-O v6.0 HBM, WorldSid-50M model v7.6 & THOR model v1.8.1) of the sled simulation cases in matrix I & II

Target	C1	C2	C3	C4	C5	C6	C7	C8	C9	C10	C11	C12	C13
	HM 134	HM 135	HM 091	HM 136	HM 137	TR 138	TR 139	TR 140	WS 141	WS 142	WS 143	WS 144	WS 145
Head Disp. Y (mm)	280.8	447.9	702.2	436.1	439.2	490.5	492.7	540.8	447.8	467.9	490.9	446.4	700.3
T1 Disp. Y (mm)	245.1	417.5	558.2	426.8	413.6	483.8	472.2	455.0	401.4	402.1	393.3	259.0	525.7
T4 Disp. Y (mm)	215.4	376.2	518.3	383.7	366.8	458.1	446.9	415.4	385.3	374.4	338.4	221.2	463.7
T12 Disp. Y (mm)	171.9	277.9	380.8	291.1	263.2	346.8	325.8	265.9	332.6	295.8	235.0	176.6	317.1
LShoulder Disp. Y (mm)	215.5	364.0	568.9	373.2	360.2	453.1	441.3	464.0	368.3	372.0	391.1	250.2	542.5
RShoulder Disp. Y (mm)	213.7	350.7	499.5	351.4	337.0	398.2	377.9	370.9	372.4	363.5	297.0	200.0	428.2
Pelvis Disp. Y (mm)	188.4	308.0	309.0	290.3	243.1	286.5	268.7	227.3	346.6	303.6	204.2	255.3	267.8
LKnee Disp. Y (mm)	294.4	563.9	495.6	526.2	387.6	526.9	375.6	365.1	700.0	703.7	543.2	792.8	790.2
RKnee Disp. Y (mm)	282.0	492.7	241.2	469.7	223.2	369.0	286.0	215.0	557.2	536.3	330.3	561.1	594.1

Appendix-C: The FMVSS214 Compact Car Pole Crash Far-side Occupant Simulation Matrix III Results

Table C-1.
Responses and injury measures of the occupant models (GHBMC AM50-O v6.0 HBM, WorldSid-50M model v7.6 & THOR model v1.8.1) of the sled simulation cases in matrix III

Body Region	*Injury Measure*	C14	C15
		HM146	WS147
Head	***HIC15***	161.25	51.25
	BrIC	0.68	0.76
Neck	***NIJ (Upper)***	0.34	0.48
	NIJ (Lower)	0.60	0.38
	Tension (Upper)	0.37	1.05
	Extension (Upper)	20.13	18.16
	Lateral Bend (Upper)	24.27	24.48
	Tension (Lower)	1.43	0.72
	Extension (Lower)	63.97	123.39
	Lateral Bend (Lower)	47.82	24.60
Thorax	***T4 G 3ms***	0.202	0.29
	L Shoulder Joint Force	0.249	0.82
	R Shoulder Joint Force	27.51	13.56
	L Shoulder Rib Def	52.28	14.24
	R Shoulder Rib Def	28.90	10.41
	L. Upper Chest Def	58.17	4.02
	R. Upper Chest Def	35.07	10.96
	L. Mid Chest Def	38.68	7.55
	L. Low Chest Def	62.05	8.99
	R. Mid Chest Def	76.54	33.99
	R Low Chest Def	30.55	3.17
Abdomen	***L Upper ABD Def***	56.09	43.95
	R Upper ABD Def	35.47	4.04
	L Low ABD Def	59.72	33.75
	R Low ABD Def	0.52	51.25
	L Upper ABD Vmax*Cmax	0.66	--
	R Upper ABD Vmax*Cmax	0.60	--
	L Low ABD Vmax*Cmax	2.20	--
	R Low ABD Vmax*Cmax	0.48	--
Pelvis	***Pubic Force***	2.19	1.48
	L. Accetab Force	2.11	2.52
	R. Accetab Force	0.51	0.41
KTH	***L. Femur Force***	0.41	0.32
	R. Femur Force	161.25	0.37

Table C-2.
Kinematics target relative displacements of the occupant models (GHBMC AM50-O v6.0 HBM, WorldSid-50M model v7.6 & THOR model v1.8.1) of the sled simulation cases in matrix III

Target	C14	C15
	WS 146	WS 147
Head Disp. Y (mm)	635.5	476.6
T1 Disp. Y (mm)	465.4	336.7
T4 Disp. Y (mm)	399.0	271.0
T12 Disp. Y (mm)	228.2	174.9
LShoulder Disp. Y (mm)	521.9	353.1
RShoulder Disp. Y (mm)	373.7	240.6
Pelvis Disp. Y (mm)	185.6	157.4
LKnee Disp. Y (mm)	261.3	243.1
RKnee Disp. Y (mm)	78.5	56.2